arXiv:1606.04117v2 [cond-mat.quant-gas] 18 Jun 2016

Space-time correlations in the Bose Hubbard model after a quantum quench

Matthew R. C. Fitzpatrick and Malcolm P. Kennett
Department of Physics, Simon Fraser University,
8888 University Drive, Burnaby, British Columbia V5A 1S6, Canada
(Dated: June 21, 2016)

We study correlations in space and time after a quantum quench in the Bose Hubbard model. We obtain a two particle irreducible effective action within the Schwinger-Keldysh formalism that allows us to study dynamics in both the superfluid and Mott insulating phases. We derive equations of motion for both the superfluid order parameter and two-point correlation functions. We discuss the numerical solutions of these equations and calculate the quasimomentum distribution for quenches in the Mott phase. We demonstrate light-cone like spreading of correlations in the Mott phase in both one and two dimensions and calculate the propagation velocity in each dimension.

PACS numbers: 37.10.Jk,03.75.Kk,05.30.Jp,05.30.Rt

I. INTRODUCTION

The out of equilibrium dynamics of cold atoms trapped in optical lattices has received considerable attention in recent years [1–5]. The ability to tune experimental parameters over a wide range of values in real time makes these systems very versatile and gives the opportunity to study quantum systems out of equilibrium in a very controlled fashion. Quantum quenches, in which parameters in the Hamiltonian are varied in time faster than the system can respond adiabatically, e.g. when a system is driven through a quantum critical point, are a protocol that is natural to study in a cold atom context and have been studied intensely both theoretically and experimentally.

The Bose Hubbard model (BHM) [6] has been shown to describe interacting ultracold bosons in an optical lattice [7], allowing the opportunity for experiments to probe the out of equilibrium dynamics of the model [7–24]. The BHM is a particularly convenient context for studying quantum quenches as it displays a quantum phase transition between the superfluid and Mott-insulator phases (or vice versa) as the ratio of intersite hopping J to the on-site repulsion U is varied, as observed by Greiner *et al.* [8]. Theoretical studies of the BHM suggest that whether equilibration occurs or not after a quantum quench depends sensitively on the initial and final values of J/U and the chemical potential [25–32]. In the case of quenches from superfluid (large J/U) to Mott insulator (small J/U) there have been suggestions that there may be aging behaviour and glassiness that might be experimentally observable in two time correlations or in violations of the fluctuation dissipation theorem [5, 25, 28–30, 32]. In the alternative quench from Mott insulator to superfluid, it has been suggested that Kibble-Zurek [33–35] scaling of defects should be observed [36, 37], which has recently been tested experimentally [22].

In experiments, the combination of a harmonic trap and small J/U leads to a wedding cake structure of the equilibrium density, reflecting alternating Mott insulating and superfluid regions [38, 39]. The presence of Mott insulating regions has been predicted to retard relaxation to equilibrium after a quench to small J/U by impeding mass transport of bosons through the insulating regions [40, 41] and has been observed experimentally [42]. This gives a picture in which relaxation after a quench takes place through a two step process – first there is fast relaxation to local equilibrium and then second, relaxation via mass transport [40, 43].

In addition to slow dynamics, several analytical and numerical studies have also shown a Lieb-Robinson-like [44] bound of a maximal velocity which leads to a light-cone like spreading of density correlations in one dimensional systems for quenches from the superfluid to Mott-insulating regime as well as quenches within the Mott-insulating regime [26, 41, 45, 46]. The latter case was recently observed experimentally by Cheneau *et al.* [47]. Similar predictions have been made for higher dimensional systems [48, 49]. The results summarized above motivate our study of the temporal and spatial correlations of the BHM after a quantum quench in order to elucidate the dynamics observed after quenches.

A generic problem in the theoretical description of quantum quenches is that it is necessary to have a formalism that is able to describe the physics in the phases on both sides of a quantum critical point. In the case of the Bose Hubbard model, numerical approaches such as exact diagonalization and the time-dependent density matrix renormalization group (t-DMRG) [23, 25, 41, 45, 47, 50, 51] can be essentially exact in all parts of parameter space but are limited by system size and usually are practical only in one dimension. For dimensions higher than one, methods such as time-dependent Gutzwiller mean field theory [3, 40, 52, 53] and dynamical mean field theory [31] have been used which can capture the presence of a quantum phase transition, but in their simplest form do not capture spatial correlations, although there has been work on including perturbative corrections [48, 54–58]. An analytical approach based on using two Hubbard Stratonovich transformations to capture both weak-coupling and strong-coupling physics in the same formalism was developed by Sengupta and Dupuis [59]. This was generalized by one of us from an equilibrium theory to out of equilibrium by using the Schwinger-

Keldysh formalism to obtain a one-particle irreducible (1PI) effective action [30].

In this paper we extend the approach developed in Ref. [30] to obtain a two-particle irreducible (2PI) effective action which allows us to derive equations of motion after a quantum quench. Our main results are i) the 2PI effective action and the equations of motion, and ii) the extraction of propagation velocities for the light-cone like spreading of correlations in the Mott phase in both one and two dimensions. The equations of motion treat the order parameter and the two-point Green's functions on the same footing and allow us to deal with correlations in the broken symmetry (superfluid) phase. We solve these equations numerically to obtain the quasi-momentum distribution in one and two dimensional systems for quenches in the Mott phase. We find that in both one and two dimensional systems there is light-cone like spreading of the single-particle correlations such that there is a propagating front with a constant velocity. We relate these results to previous theoretical and experimental studies.

This paper is structured as follows. In Sec. II, we describe the model that we study and derive the 2PI effective action for the BHM. In Sec. III, we obtain the equations of motion for both the order parameter and the two-particle Green's function by taking appropriate variations of the 2PI effective action. In Sec. IV, we present numerical results obtained from integrating the equations of motion and finally in Sec. V we discuss our results and present our conclusions.

II. MODEL AND FORMALISM

In this section we introduce the Bose Hubbard model and discuss the generalization of the 1PI approach developed in Ref. [30] to a 2PI effective action within the Schwinger-Keldysh formalism. The Hamiltonian for the BHM, allowing for a time dependent hopping term, is given by

$$\hat{H}_{\rm BH}(t) = \hat{H}_J(t) + \hat{H}_0, \tag{1}$$

where

$$\hat{H}_J(t) = -\sum_{\langle i,j\rangle} J_{ij}(t)\left(\hat{a}_i^\dagger \hat{a}_j + \hat{a}_j^\dagger \hat{a}_i\right), \tag{2}$$

$$\hat{H}_0 = \hat{H}_U - \mu\hat{N} = \tfrac{U}{2}\sum_j \hat{n}_j\left(\hat{n}_j - 1\right) - \mu\sum_j \hat{n}_j, \tag{3}$$

with $\hat{a}_i^\dagger$ and $\hat{a}_i$ annihilation and creation operators for bosons on site i respectively, $\hat{n}_i \equiv \hat{a}_i^\dagger \hat{a}_i$ the number operator, U the interaction strength, and μ the chemical potential. The notation $\langle i,j\rangle$ indicates a sum over nearest neighbours only. We allow $J_{ij}(t)$, the hopping amplitude between sites i and j, to be time dependent.

A. Schwinger-Keldysh technique

We use the Schwinger-Keldysh [60, 61] or closed-time-path (CTP) technique [62–65], which is formulated in real-time, unlike the imaginary-time Matsubara formalism, which is restricted to equilibrium, to describe the out-of-equilibrium behaviour of the BHM. The trade-off for using the CTP technique is that the number of fields in the theory doubles. For every field propagating forward in time, there is a second copy propagating backwards in time. As a result, when calculating Green's functions, the notion of time ordering needs to be replaced by that of contour ordering [63]. The choice of the contour depends on the problem of interest. Assuming a thermal initial state in our case, we work with a contour of the form illustrated in Fig. 1, where for simplicity we set $\sigma = 0$. A number of authors have applied

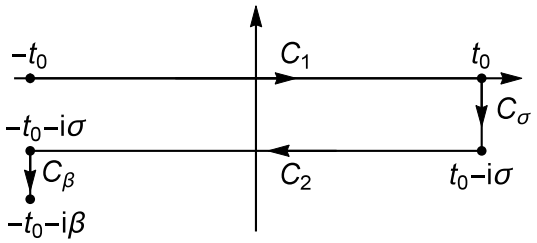

FIG. 1. Contour for the Schwinger-Keldysh technique for a system with inverse temperature β. The value of σ is arbitrary in the interval $[0, \beta]$ (Ref. [64]).

CTP approaches to the BHM [30, 66–74] – our work differs from previous approaches in that we develop a 2PI approach within the CTP formalism that is appropriate for strong coupling as well as weak coupling [70, 72].

B. Green's functions and the 1PI Generating functionals

To characterize spatio-temporal correlations in the BHM we calculate contour-ordered Green's functions (COGFs). We generalize the work in Ref. [30] to include Green's functions with unequal numbers of annihilation and creation operators to allow for the study of broken symmetry phases. We frequently use the compact notation $\hat{a}_i^a$ for the bosonic fields, defined by

$$\hat{a}_i^1 \equiv \hat{a}_i, \quad \hat{a}_i^2 \equiv \hat{a}_i^\dagger. \tag{4}$$

Following Chou *et al.* [65], we define the n-point COGF as

$$\begin{aligned} &G^{a_1,\ldots,a_n}_{r_1,\ldots,r_n}(\tau_1,\ldots,\tau_n) \\ &\quad\equiv (-i)^{n-1}\mathrm{Tr}\left\{\hat{\rho}_0\, T_C\left[\hat{a}^{a_1}_{r_1}(\tau_1)\ldots\hat{a}^{a_n}_{r_n}(\tau_n)\right]\right\} \\ &\quad\equiv (-i)^{n-1}\left\langle T_C\left[\hat{a}^{a_1}_{r_1}(\tau_1)\ldots\hat{a}^{a_n}_{r_n}(\tau_n)\right]\right\rangle_{\rho_0}, \end{aligned} \tag{5}$$

where $\hat{\rho}_0$ is the state operator describing a thermal initial state

$$\hat{\rho}_0 = \frac{e^{-\beta \hat{H}_0}}{\mathrm{Tr}\left\{e^{-\beta \hat{H}_0}\right\}}, \tag{6}$$

and $\hat{a}^a_r(\tau)$ are the bosonic fields in the Heisenberg picture with respect to $\hat{H}_{\rm BH}(t)$ [Eq. (1)]. Here we have introduced explicitly the complex contour time argument τ along with the contour time ordering operator T_C, which orders strings of operators according to their position on the contour, with operators at earlier contour times placed to the right. Note that the presence of T_C in Eq. (5) leads to the following symmetry property of the COGFs

$$G^{a_1,\ldots,a_n}_{r_1,\ldots,r_n}(\tau_1,\ldots,\tau_n) = G^{a_{p_1},\ldots,a_{p_n}}_{r_{p_1},\ldots,r_{p_n}}(\tau_{p_1},\ldots,\tau_{p_n}), \tag{7}$$

where $\{p_1,\ldots,p_n\}$ is any permutation of the sequence $\{1,\ldots,n\}$.

We restrict ourselves to contour times residing on either the forward C_1 or backward C_2 parts of the contour in Fig. 1 (with $\sigma = 0$) when calculating the COGFs. This allows us to rewrite the bosonic fields $\hat{a}^a_r(\tau)$ as

$$\hat{a}^a_r(\tau) = \hat{a}^a_{r,\alpha}(t), \tag{8}$$

where t is a real-time argument and $\alpha = 1, 2$ is the Keldysh index, which indicates whether a field is on the forward or backward part of the contour. The combination (α, t) uniquely specifies τ. Using Eq. (8), we can rewrite the COGFs in Eq. (5) as

$$\begin{aligned} &G^{a_1,\ldots,a_n}_{r_1,\ldots,r_n,\alpha_1,\ldots,\alpha_n}(t_1,\ldots,t_n) \\ &\quad\equiv (-i)^{n-1}\mathrm{Tr}\left\{\hat{\rho}_0\, T_C\left[\hat{a}^{a_1}_{r_1,\alpha_1}(t_1)\ldots\hat{a}^{a_n}_{r_n,\alpha_n}(t_n)\right]\right\} \\ &\quad\equiv (-i)^{n-1}\left\langle T_C\left[\hat{a}^{a_1}_{r_1,\alpha_1}(t_1)\ldots\hat{a}^{a_n}_{r_n,\alpha_n}(t_n)\right]\right\rangle_{\rho_0}. \end{aligned} \tag{9}$$

The COGFs above can be derived from a generating functional $\mathcal{Z}[f]$ defined as

$$\begin{aligned} \mathcal{Z}[f] &\equiv \mathrm{Tr}\left\{\hat{\rho}_0\, T_C\left[e^{i\int_C d\tau \sum_i f^{\overline{a}}_i(\tau)\hat{a}^a_i(\tau)}\right]\right\} \\ &= \mathrm{Tr}\left\{\hat{\rho}_0\, T_C\left[e^{i\left(\int_{C_1}+\int_{C_2}+\int_{C_\beta}\right)d\tau\sum_i f^{\overline{a}}_i(\tau)\hat{a}^a_i(\tau)}\right]\right\} \\ &= \mathrm{Tr}\left\{\hat{\rho}_0\, T_C\left[e^{i\int_{-t_0}^{t_0} dt\sum_i f^{\overline{a}}_{i,\alpha}(t)\tau^3_{\alpha\beta}\hat{a}^a_{i,\beta}(t)}\right.\right. \\ &\qquad\left.\left.\times e^{i\int_{C_\beta} d\tau\sum_i f^{\overline{a}}_i(\tau)\hat{a}^a_i(\tau)}\right]\right\}, \end{aligned} \tag{10}$$

where the fs are source currents, σ^i is the $i^{\rm th}$ Pauli matrix acting on the superscripts of the fields (e.g. a, b), τ^i is the $i^{\rm th}$ Pauli matrix acting on the subscript Keldysh indices (e.g. α, β), and the overscored index in $f^{\overline{a}}_{i,\alpha}(t)$ is defined by

$$f^{\overline{a}}_{i,\alpha}(t) = \sigma^{ab}_1 f^b_{i,\alpha}(t), \tag{11}$$

i.e. $\overline{1} = 2$ and $\overline{2} = 1$. It is clear from the definition above that the generating functional is normalized such that $\mathcal{Z}[0] = 1$.

To derive the COGFs in Eq. (9) from $\mathcal{Z}[f]$, we take appropriate functional derivatives with respect to the sources and set the sources to zero afterwards

$$\begin{aligned} &G^{a_1,\ldots,a_n}_{r_1,\ldots,r_n,\alpha_1,\ldots,\alpha_n}(t_1,\ldots,t_n) \\ &\quad\equiv i(-1)^n\tau^3_{\alpha_1\beta_1}\ldots\tau^3_{\alpha_n\beta_n} \\ &\qquad\times\frac{1}{\mathcal{Z}[0]}\left.\frac{\delta^n\mathcal{Z}[f]}{\delta f^{\overline{a}_1}_{r_1,\beta_1}(t_1)\ldots\delta f^{\overline{a}_n}_{r_n,\beta_n}(t_n)}\right|_{f=0} \end{aligned}$$

To this point, our discussion of the COGFs and $\mathcal{Z}[f]$ has been quite general – we now discuss the BHM specifically.

C. Path integral form of $\mathcal{Z}[f]$ for the BHM

We cast the COGFs and the generating functional $\mathcal{Z}[f]$ in path integral form [63], which for the case of the BHM is [30]

$$\mathcal{Z}[f] = \int [\mathcal{D}a^a] e^{iS_{\rm BHM}[a]+iS_f[a]}, \tag{12}$$

where $S_{\rm BHM}$ is the action for the BHM, and $\int[\mathcal{D}a^a]$ is the coherent-state measure. We absorb overall constants into the measure as they will cancel out in the calculation of the COGFs due to the factor of $1/\mathcal{Z}[0]$ in Eq. (12). Note that in the path-integral formalism $a^1_{i,\alpha} = a_{i,\alpha}$ and $a^2_{i,\alpha} = a^*_{i,\alpha}$.

In the limit that $t_0 \to -\infty$, if the initial state (at infinitely early times) is thermalized, then the generating functional may be factorized [63]

$$\mathcal{Z} = \mathcal{Z}_{C_1\cup C_2}\mathcal{Z}_{C_\beta}, \tag{13}$$

and we can ignore $\mathcal{Z}_{C_\beta}$ when focusing on real time dynamics [62]. This allows the COGFs to be written as

$$\begin{aligned} &\left\langle T_C\left[\hat{a}^{a_1}_{r_1,\alpha_1}(t_1)\ldots\hat{a}^{a_n}_{r_n,\alpha_n}(t_n)\right]\right\rangle_{\rho_0} \\ &\qquad\equiv\left\langle a^{a_1}_{r_1,\alpha_1}(t_1)\ldots a^{a_n}_{r_n,\alpha_n}(t_n)\right\rangle_{S_{\rm BHM}}. \end{aligned} \tag{14}$$

Contour ordering, which was explicit for the operator representation is implicit in the path integral representation [75]. In addition to the generating functional, we make extensive use of the generator of connected COGFs (CCOGFs) defined by

$$W[f] = -i\ln\mathcal{Z}[f]. \tag{15}$$

The n-point CCOGFs $G^{a_1,\ldots,a_n,c}_{r_1,\ldots,r_n,\alpha_1,\ldots,\alpha_n}(t_1,\ldots,t_n)$ can be obtained from $W[f]$ by calculating

$$\begin{aligned} &G^{a_1,\ldots,a_n,c}_{r_1,\ldots,r_n,\alpha_1,\ldots,\alpha_n}(t_1,\ldots,t_n) \\ &\quad\equiv(-1)^{n-1}(\tau^3_{\alpha_1\beta_1}\ldots\tau^3_{\alpha_n\beta_n}) \\ &\qquad\times\left.\frac{\delta^n W[f]}{\delta f^{\overline{a}_1}_{r_1,\beta_1}(t_1)\ldots\delta f^{\overline{a}_n}_{r_n,\beta_n}(t_n)}\right|_{f=0} \\ &\quad=(-i)^{n-1}\left\langle a^{a_1}_{r_1,\alpha_1}(t_1)\ldots a^{a_n}_{r_n,\alpha_n}(t_n)\right\rangle^c_{S_{\rm BHM}}, \end{aligned} \tag{16}$$

where $\langle \ldots \rangle^c$ indicates that only connected diagrams are kept. Note that the CCOGFs satisfy the same symmetry property as the COGFs

$$G^{a_1,\ldots,a_n,c}_{r_1,\ldots,r_n,\alpha_1,\ldots,\alpha_n}(t_1,\ldots,t_n) = G^{a_{p_1},\ldots,a_{p_n},c}_{r_{p_1},\ldots,r_{p_n},\alpha_{p_1},\ldots,\alpha_{p_n}}(t_{p_1},\ldots,t_{p_n}). \quad (17)$$

D. Keldysh Rotation

For the n-point CCOGF defined in Eq. (16) there are 2^n Keldysh components. However, as a consequence of causality, for any n there is at least one component which is not independent of the others [65]. We can eliminate one of these components by performing a $\pi/4$-rotation in Keldysh space [61], which transforms the bosonic fields

$$\begin{pmatrix} a_1(t) \\ a_2(t) \end{pmatrix} \longrightarrow \begin{pmatrix} \tilde{a}_q(t) \\ \tilde{a}_c(t) \end{pmatrix} = \hat{L} \begin{pmatrix} a_1(t) \\ a_2(t) \end{pmatrix}, \quad (18)$$

with

$$\hat{L} = \frac{1}{\sqrt{2}} \begin{pmatrix} 1 & -1 \\ 1 & 1 \end{pmatrix}, \quad (19)$$

where $\tilde{a}_q$ and $\tilde{a}_c$ are the quantum and classical components of the field, respectively [69, 76–78]. As a consequence of the above basis transformation $(1,2) \to (q,c)$, the matrix $\tau^3 \to \tau^1$, and the rotated version of the BHM action takes the form [30] (dropping tildes)

$$S_{\rm BHM} = \int_{-\infty}^{\infty} dt \sum_i [a^*_{i\overline{\alpha}}(t)(i\partial_t)a_{i\alpha}(t)] + S_U + S_J, \quad (20)$$

where

$$S_U = \int_{-\infty}^{\infty} dt \sum_i \left[a^*_{i\alpha}(t)a_{i\alpha}(t)a^*_{i\overline{\beta}}(t)a_{i\beta}(t) \right], \quad (21)$$

$$S_J = \int_{-\infty}^{\infty} dt \sum_{\langle i,j \rangle} J_{ij} \left[a^*_{i\overline{\alpha}}(t)a_{j\alpha}(t) + a^*_{j\overline{\alpha}}(t)a_{i\alpha}(t) \right], \quad (22)$$

and

$$S_f = \int_{-\infty}^{\infty} dt \sum_i f^{\overline{a}}_{i,\overline{\alpha}}(t)a^a_{i,\alpha}(t), \quad (23)$$

where we made use of the overscored notation on the Keldysh indices. In the (q,c) basis, the CCOGFs are generated by calculating

$$G^{a_1,\ldots,a_n,c}_{r_1,\ldots,r_n,\alpha_1,\ldots,\alpha_n}(t_1,\ldots,t_n) \equiv (-1)^{n-1} \left. \frac{\delta^n W[f]}{\delta f^{\overline{a}_1}_{r_1,\overline{\alpha}_1}(t_1)\ldots\delta f^{\overline{a}_n}_{r_n,\overline{\alpha}_n}(t_n)} \right|_{f=0}. \quad (24)$$

E. 1PI action for the Bose-Hubbard model

In order to study quench dynamics in the BHM, we make use of an effective theory that can describe both the weak and strong coupling limits of the model in the same formalism. Such an approach was developed in imaginary time by Sengupta and Dupuis [59] by using two Hubbard-Stratonovich transformations and generalized to real time in Ref. [30]. A similar real-time theory was also obtained based on a Ginzburg-Landau approach using the CTP technique [67–69]. A brief discussion of the derivation of the 1PI action along with minor corrections to several expressions presented in Ref. [30] is given in Appendix A. The 1PI action obtained in Ref. [30] for z fields (which are obtained after two Hubbard Stratonovich transformations and have the same correlations as the original a fields [59]) is

$$S^{\rm 1PI}_{\rm BHM} = \int_{-\infty}^{\infty} dt \sum_{ij} 2J_{ij}(t) z^*_{i\overline{\alpha}}(t) z_{j\alpha}(t) + \int_{-\infty}^{\infty} dt_1 dt'_1 \sum_{ij} z^*_{i\alpha_1}(t_1)\delta_{ij} \left[\mathcal{G}^{1,c}\right]^{-1}_{\alpha_1\alpha'_1}(t_1,t'_1) z_{j\alpha'_1}(t'_1) + \frac{1}{4}\int_{-\infty}^{\infty} dt_1 dt_2 dt'_1 dt'_2 \sum_i u_{\alpha_1\alpha_2\alpha'_1\alpha'_2}(t_1,t_2,t'_1,t'_2) z^*_{i\alpha_1}(t_1) z^*_{i\alpha_2}(t_2) z_{i\alpha'_1}(t'_1) z_{i\alpha'_2}(t'_2), \quad (25)$$

where $\left[\mathcal{G}^{1,c}\right]^{-1}_{\alpha_1\alpha'_1}(t_1,t'_1)$ is the inverse of the single site connected Green's function (see Appendix A for the definition of $\mathcal{G}^{n,c}$) and $u_{\alpha_1\alpha_2\alpha'_1\alpha'_2}(t_1,t_2,t'_1,t'_2)$ is the local four-point vertex function

$$u_{\alpha_1\alpha_2\alpha'_1\alpha'_2}(t_1,t_2,t'_1,t'_2) = -\int_{-\infty}^{\infty} dt_3 dt_4 dt'_3 dt'_4 \left[\mathcal{G}^{1,c}\right]^{-1}_{\alpha_1\alpha_3}(t_1,t_3) \left[\mathcal{G}^{1,c}\right]^{-1}_{\alpha_2\alpha_4}(t_2,t_4) \times \mathcal{G}^{2,c}_{\alpha_3\alpha_4\alpha'_3\alpha'_4}(t_3,t_4,t'_3,t'_4) \left[\mathcal{G}^{1,c}\right]^{-1}_{\alpha'_3\alpha'_1}(t'_3,t'_1) \left[\mathcal{G}^{1,c}\right]^{-1}_{\alpha'_4\alpha'_2}(t'_4,t'_2), \quad (26)$$

both of which are independent of site index i, hence we write them without site labels (the site labels are retained in the derivation given in Appendix A), although it is

straightforward to include them if for instance one considers the BHM with a harmonic potential as is realised experimentally.

The Keldysh structure of $\left[\mathcal{G}^{1,c}\right]^{-1}_{\alpha\alpha'}(t,t')$ is given by

$$\begin{aligned}
\left[\mathcal{G}^{1,c}\right]^{-1}_{qq}(t,t') &= -\int_{-\infty}^{\infty} dt''dt''' \left[\mathcal{G}^{R}\right]^{-1}(t,t'') \\
&\quad \times \mathcal{G}^{K}(t'',t''') \left[\mathcal{G}^{A}\right]^{-1}(t''',t'), \\
\left[\mathcal{G}^{1,c}\right]^{-1}_{qc}(t,t') &= \left[\mathcal{G}^{R}\right]^{-1}(t,t'), \\
\left[\mathcal{G}^{1,c}\right]^{-1}_{cq}(t,t') &= \left[\mathcal{G}^{A}\right]^{-1}(t,t'), \\
\left[\mathcal{G}^{1,c}\right]^{-1}_{cc}(t,t') &= 0,
\end{aligned} \tag{27}$$

where the $\mathcal{G}^{R,A,K}(t,t')$ are retarded, advanced and Keldysh local Green's functions respectively [30] which are defined as:

$$\begin{aligned}
i\mathcal{G}^{K}(t,t') &= i\mathcal{G}^{<}(t,t') + i\mathcal{G}^{>}(t,t'), \\
i\mathcal{G}^{R}(t,t') &= \theta(t-t')[i\mathcal{G}^{>}(t,t') - i\mathcal{G}^{<}(t,t')], \\
i\mathcal{G}^{A}(t,t') &= \theta(t'-t)[i\mathcal{G}^{<}(t,t') - i\mathcal{G}^{>}(t,t')],
\end{aligned}$$

with

$$\begin{aligned}
i\delta_{ij}\mathcal{G}^{<}(t,t') &= \langle \hat{a}_i^*(t')\hat{a}_j(t)\rangle_{\rho_0}, \\
i\delta_{ij}\mathcal{G}^{>}(t,t') &= \left\langle \hat{a}_i(t)\hat{a}_j^*(t')\right\rangle_{\rho_0}.
\end{aligned}$$

Note that the local Green's functions are time translation invariant:

$$\mathcal{G}^{R,A,K}(t,t') = \mathcal{G}^{R,A,K}(t-t'). \tag{28}$$

Equation (25) is the key result from Ref. [30] that we use to develop the 2PI formalism in Sec. II F. This action gives the exact two-point CCOGF in both the local ($J_{ij}=0$) and noninteracting ($U=0$) limits [59, 79]. This feature makes this theory particularly appealing for the study of quench dynamics, since it gives the hope that one can accurately describe the behaviour of the system in both superfluid and Mott-insulating regimes [5]. Furthermore, the action in Eq. (25) also leads to the correct mean-field phase boundary [30].

Lastly, using the symmetry relation in Eq. (A8), we see that the four-point vertex u satisfies the symmetry relation (correcting Ref. [30])

$$\begin{aligned}
u_{\alpha_1\alpha_2\alpha_1'\alpha_2'}(t_1,t_2,t_1',t_2') &= u_{\alpha_2\alpha_1\alpha_1'\alpha_2'}(t_2,t_1,t_1',t_2') \\
&= u_{\alpha_1\alpha_2\alpha_2'\alpha_1'}(t_1,t_2,t_2',t_1').
\end{aligned} \tag{29}$$

Similar symmetry relations of four-point functions were noted in Refs. [5, 68, 69].

F. 2PI Formalism and the effective action $\Gamma(\phi, G)$

In order to obtain the full two-point CCOGF (the "full propagator" from now on), which encodes non-local spatial and temporal correlations, we adopt a two particle irreducible (2PI) approach. Unlike 1PI approaches [30, 59, 67–69], the 2PI formalism describes the evolution of the mean field (i.e. superfluid order parameter for the BHM) and the full propagator on equal footing [70]. Several authors [70, 72] have applied the 2PI formalism to the BHM to derive equations of motion for the mean field and the full propagator for weak interactions. These equations of motion were also used to derive a quantum kinetic equation [71].

Here, we develop a real-time 2PI approach based on the strong-coupling theory of Sengupta and Dupuis [30, 59] to capture behaviour of correlations across a quantum quench. We adopt a compact notation where we write an arbitrary function A of times t_i, with site indices $i,j,k,\ldots$, Keldysh indices α_i and upper indices a_i as

$$A^{a_1\ldots a_n}_{i_1\ldots i_n,\alpha_1\ldots\alpha_n}(t_1\ldots t_n) = A^{a_1\ldots a_n}_{i_1\ldots i_n,x_1\ldots x_n}. \tag{30}$$

We use the Einstein summation convention for all indices except site indices, where summations are written explicitly. Sums over time variables are to be understood as integrals from $t=-\infty$ to $t=\infty$.

We can rewrite Eq. (25) in condensed notation as

$$\begin{aligned}
S[z] = \sum_{ij} z^{a_1}_{i,x_1}\left(-\frac{1}{2!}\left[g_0^{-1}\right]^{a_1a_2}_{ij,x_1x_2}\right) z^{a_2}_{j,x_2} \\
+ \frac{1}{4!} g^{a_1a_2a_3a_4}_{x_1x_2x_3x_4} \sum_i z^{a_1}_{i,x_1} z^{a_2}_{i,x_2} z^{a_3}_{i,x_3} z^{a_4}_{i,x_4},
\end{aligned} \tag{31}$$

where we have introduced the generalized inverse bare propagator $\left[g_0^{-1}\right]^{a_1a_2}_{ij,x_1x_2}$

$$\begin{aligned}
\left[g_0^{-1}\right]^{a_1a_2}_{ij,x_1x_2} &= -\delta_{ij}\left[\mathcal{G}^{-1}\right]^{a_1a_2}_{\alpha_1\alpha_2}(t_1,t_2) \\
&\quad - 2\sigma_1^{a_1a_2} J_{ij}(t_1)\tau^1_{\alpha_1\alpha_2}\delta(t_1-t_2),
\end{aligned} \tag{32}$$

where $\left[\mathcal{G}^{-1}\right]^{a_1a_2}_{\alpha_1\alpha_2}(t_1,t_2)$ is non-zero only for $a_1\neq a_2$, and the components can be related to $\left[\mathcal{G}^{1,c}\right]^{-1}_{\alpha_1\alpha_2}(t_1,t_2)$ which was specified in Sec. II E. In particular, note that

$$\left[\mathcal{G}^{-1}\right]^{a_1a_2}_{\alpha_1\alpha_2}(t_1,t_2) = \begin{cases} 0, & a_1 = a_2 \\ \left[\mathcal{G}^{a_2a_1}\right]^{-1}_{\alpha_1\alpha_2}(t_1,t_2), & a_1\neq a_2 \end{cases}. \tag{33}$$

We also introduce the generalized local four-point vertex function $g^{a_1a_2a_3a_4}_{x_1x_2x_3x_4}$

$$\begin{aligned}
g^{a_1a_2a_3a_4}_{x_1x_2x_3x_4} \equiv -\left[\mathcal{G}^{-1}\right]^{a_1a_5}_{x_1x_5}\left[\mathcal{G}^{-1}\right]^{a_2a_6}_{x_2x_6}\mathcal{G}^{a_5a_6a_7a_8}_{x_5x_6x_7x_8} \\
\times\left[\mathcal{G}^{-1}\right]^{a_7a_3}_{x_7x_3}\left[\mathcal{G}^{-1}\right]^{a_8a_4}_{x_8x_4}.
\end{aligned} \tag{34}$$

The permutation symmetry of the indices of CCOGFs implies that

$$\left[g_0^{-1}\right]^{a_1a_2}_{x_1x_2} = \left[g_0^{-1}\right]^{a_2a_1}_{x_2x_1}, \tag{35}$$

$$g^{a_1a_2a_3a_4}_{x_1x_2x_3x_4} = g^{a_{P_1}a_{P_2}a_{P_3}a_{P_4}}_{x_{P_1}x_{P_2}x_{P_3}x_{P_4}}, \tag{36}$$

and that the only non-zero value of the four point vertex is (up to permutations)

$$g^{2,2,1,1}_{x_1x_2x_3x_4} = u_{\alpha_1\alpha_2\alpha_3\alpha_4}(t_1,t_2,t_3,t_4). \tag{37}$$

In the 2PI formalism [80, 81], physical quantities are expressed in terms of the mean field ϕ and the full propagator G

$$\phi^{a_1}_{i,x_1} \equiv \left\langle z^{a_1}_{i,x_1} \right\rangle, \tag{38}$$

$$iG^{a_1a_2}_{ij,x_1x_2} \equiv \left\langle z^{a_1}_{i,x_1} z^{a_2}_{j,x_2} \right\rangle - \left\langle z^{a_1}_{i,x_1} \right\rangle \left\langle z^{a_2}_{j,x_2} \right\rangle. \tag{39}$$

Note that by definition, G is symmetric $G^{a_1a_2}_{ij,x_1x_2} = G^{a_2a_1}_{ji,x_2x_1}$. The equations of motion for ϕ and G are obtained by requiring the 2PI effective action $\Gamma[\phi,G]$ be stationary with respect to variations of ϕ and G. This is similar to the 1PI case where the equations of motion for ϕ are obtained by requiring the 1PI effective action $\Gamma[\phi]$ to be stationary with respect to variations of ϕ. The full propagator from the 2PI effective action allows one to take into account broken symmetry states [80, 81], which is important when considering quenches in the superfluid regime.

To obtain the effective action we define the 2PI generating functional for Green's functions $\mathcal{Z}[f,K]$

$$\mathcal{Z}[f,K] = e^{iW[f,K]} = \int [\mathcal{D}z^a] e^{iS[z] + i\sum_i z^{a_1}_{i,x_1} f^{a_1}_{i,x_1} + \frac{i}{2}\sum_{ij} z^{a_1}_{i,x_1} K^{a_1a_2}_{ij,x_1x_2} z^{a_2}_{j,x_2}}, \tag{40}$$

where in addition to the single-particle source current f, we have included a (symmetric) two-particle source current K. Note that ϕ and G are obtained by calculating the following functional derivatives of $W[f,K]$:

$$\phi^{a_1}_{i,x_1} = \frac{\delta W[f,K]}{\delta f^{a_1}_{i,x_1}}, \qquad \frac{1}{2}\left(\phi^{a_1}_{i,x_1}\phi^{a_2}_{j,x_2} + iG^{a_1a_2}_{ij,x_1x_2}\right) = \frac{\delta W[f,K]}{\delta K^{a_1a_2}_{ij,x_1x_2}}.$$

These equations implicitly give f and K as functions of ϕ and G: $f = f[\phi,G]$ and $K = K[\phi,G]$. The 2PI effective action $\Gamma[\phi,G]$ is formally defined as the double Legendre transform of $W[f,K]$

$$\Gamma[\phi,G] = W[f,K] - \textstyle\sum_i f^{a_1}_{i,x_1}\phi^{a_1}_{i,x_1} - \frac{1}{2}\sum_{ij}\phi^{a_1}_{i,x_1}K^{a_1a_2}_{ij,x_1x_2}\phi^{a_2}_{j,x_2} - \frac{1}{2}\sum_{ij}K^{a_1a_2}_{ij,x_1x_2}G^{a_1a_2}_{ij,x_1x_2}, \tag{41}$$

where f and K should be understood as being expressed in terms of ϕ and G. The following identities can be derived [80] from Eq. (41)

$$\frac{\delta\Gamma[\phi,G]}{\delta\phi^{a_1}_{i,x_1}} = -f^{a_1}_{i,x_1} - \sum_j K^{a_1a_2}_{ij,x_1x_2}\phi^{a_2}_{j,x_2}, \tag{42}$$

$$\frac{\delta\Gamma[\phi,G]}{\delta G^{a_1a_2}_{ij,x_1x_2}} = -\frac{1}{2}K^{a_1a_2}_{ij,x_1x_2}. \tag{43}$$

The effective action can be shown to take the form [80, 81]

$$\Gamma[\phi,G] = S[\phi] + \frac{i}{2}\mathrm{Tr}\left\{\ln G^{-1}\right\} + \frac{i}{2}\mathrm{Tr}\left\{D^{-1}G\right\} + \Gamma_2[\phi,G] - \frac{i}{2}\mathrm{Tr}\left\{\hat{1}\right\}, \tag{44}$$

where

$$\left[D^{-1}\right]^{a_1a_2}_{ij,x_1x_2} \equiv \frac{\delta^2 S[\phi]}{\delta\phi^{a_1}_{i,x_1}\delta\phi^{a_2}_{j,x_2}} = -\left[g_0^{-1}\right]^{a_1a_2}_{ij,x_1x_2} + \frac{1}{2!}\delta_{ij}g^{a_1a_2a_3a_4}_{x_1x_2x_3x_4}\phi^{a_3}_{i,x_3}\phi^{a_4}_{i,x_4}, \tag{45}$$

and $\Gamma_2[\phi,G]$ is the sum of all 2PI connected vacuum diagrams in the theory with vertices determined by the action

$$S_{\mathrm{int}}[z;\phi] = g^{a_1a_2a_3a_4}_{x_1x_2x_3x_4}\left[\frac{1}{3!}\sum_i z^{a_1}_{i,x_1}z^{a_2}_{i,x_2}z^{a_3}_{i,x_3}\phi^{a_4}_{i,x_4} + \frac{1}{4!}\sum_i z^{a_1}_{i,x_1}z^{a_2}_{i,x_2}z^{a_3}_{i,x_3}z^{a_4}_{i,x_4}\right], \tag{46}$$

and propagator lines determined by G.

The diagrammatic expansion of $\Gamma_2[\phi,G]$ is shown in Fig. 2 up to second-order in the four-point vertex g. The

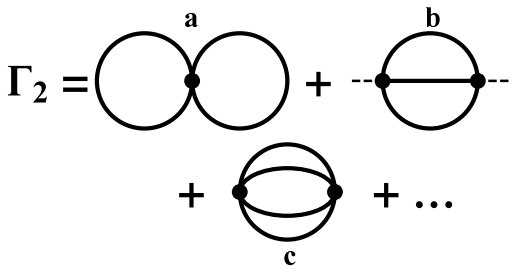

FIG. 2. Diagrammatic expansion of Γ_2 up to second-order in the four-point vertex g (shown as a solid dot) showing (a) the *double-bubble* diagram, (b) the *setting sun* diagram, and (c) the *basketball* diagram.

solid dots represent the interaction vertices g, the solid lines represent G, and the dashed lines represent ϕ (as illustrated in Fig. 3). We consider the same diagrams as discussed in Refs. [70, 72] where the BHM was studied at weak coupling. However, there is an important distinction between the two calculations, which is that the interaction vertices in Refs. [70, 72] were local in both space and time, whereas the interaction vertices we consider are local in space but *nonlocal* in time – this leads to additional features in the equations of motion that we derive.

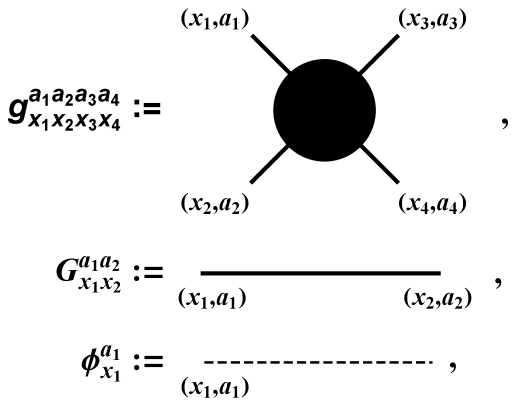

FIG. 3. The diagrammatic representation of $g^{a_1a_2a_3a_4}_{x_1x_2x_3x_4}$, $G^{a_1a_2}_{x_1x_2}$, and $\phi^{a_1}_{x_1}$.

The contributions from the three diagrams are:
i) the double–bubble (D.B.)

$$\Gamma_2^{(\mathrm{D.B.})} = -\frac{1}{8} g^{a_1a_2a_3a_4}_{x_1x_2x_3x_4} \sum_i G^{a_1a_2}_{ii,x_1x_2} G^{a_3a_4}_{ii,x_3x_4}, \tag{47}$$

ii) the setting–sun (S.S)

$$\Gamma_2^{(\mathrm{S.S.})} = \frac{1}{12} g^{a_1a_2a_3a_4}_{x_1x_2x_3x_4} g^{a_5a_6a_7a_8}_{x_5x_6x_7x_8} \sum_{ij} G^{a_1a_5}_{ij,x_1x_5} G^{a_2a_6}_{ij,x_2x_6} \times G^{a_3a_7}_{ij,x_3x_7} \phi^{a_4}_{i,x_4} \phi^{a_8}_{j,x_8}, \tag{48}$$

and iii) the basketball (B)

$$\Gamma_2^{(\mathrm{B})} = \frac{i}{48} g^{a_1a_2a_3a_4}_{x_1x_2x_3x_4} g^{a_5a_6a_7a_8}_{x_5x_6x_7x_8} \sum_{ij} G^{a_1a_5}_{ij,x_1x_5} G^{a_2a_6}_{ij,x_2x_6} \times G^{a_3a_7}_{ij,x_3x_7} G^{a_4a_8}_{ij,x_4x_8}. \tag{49}$$

III. EQUATIONS OF MOTION

To calculate the equations of motion, first we use Eqs. (42) and (43) and set the sources to zero, which gives

$$\frac{\delta S}{\delta \phi^a_{i,x}} + \frac{1}{2}\left[i \sum_{jk} \frac{\delta \left[D^{-1}\right]^{a_1a_2}_{jk,x_1x_2}}{\delta \phi^a_{i,x}} G^{a_2a_1}_{kj,x_2x_1} \right] + \frac{\delta \Gamma_2}{\delta \phi^a_{i,x}} = 0, \tag{50}$$

and

$$i\left[G^{-1}\right]^{ab}_{ij,xy} = i\left[D^{-1}\right]^{ab}_{ij,xy} - i\Sigma^{ab}_{ij,xy}, \tag{51}$$

where the second equation is Dyson's equation with

$$\Sigma^{ab}_{ij,xy} \equiv 2i \frac{\delta \Gamma_2}{\delta G^{ab}_{ij,xy}}, \tag{52}$$

the self energy. We approximate the self-energy with the contributions from the three diagrams shown in Fig. 2, so we may write

$$\Sigma \approx \Sigma^{(\mathrm{D.B.})} + \Sigma^{(\mathrm{S.S.})} + \Sigma^{(\mathrm{B})}, \tag{53}$$

and use Eqs. (47)–(49) to obtain

$$\left[\Sigma^{(\mathrm{D.B.})}\right]^{a_1a_2}_{ij,x_1x_2} = -\frac{i}{2}\delta_{ij} g^{a_1a_2a_3a_4}_{x_1x_2x_3x_4} G^{a_3a_4}_{ii,x_3x_4}, \tag{54}$$

$$\left[\Sigma^{(\mathrm{S.S.})}\right]^{a_1a_2}_{ij,x_1x_2} = \frac{i}{2} g^{a_1a_3a_4a_5}_{x_1x_3x_4x_5} g^{a_2a_6a_7a_8}_{x_2x_6x_7x_8} G^{a_3a_6}_{ij,x_3x_6} \times G^{a_4a_7}_{ij,x_4x_7} \phi^{a_5}_{i,x_5} \phi^{a_8}_{j,x_8}, \tag{55}$$

$$\left[\Sigma^{(\mathrm{B})}\right]^{a_1a_2}_{ij,x_1x_2} = -\frac{1}{6} g^{a_1a_3a_4a_5}_{x_1x_3x_4x_5} g^{a_2a_6a_7a_8}_{x_2x_6x_7x_8} G^{a_3a_6}_{ij,x_3x_6} \times G^{a_4a_7}_{ij,x_4x_7} G^{a_5a_8}_{ij,x_5x_8}. \tag{56}$$

Approximating Γ_2 with the double-bubble, setting sun and basketball diagrams, and acting with G on both sides of Eq. (51) we obtain the following equations of motion for ϕ and G:

$$0 = -\sum_j \left[g_0^{-1}\right]^{a_1a_2}_{ij,x_1x_2}\phi^{a_2}_{j,x_2} + \frac{1}{2}g^{a_1a_2a_3a_4}_{x_1x_2x_3x_4}\left(\frac{1}{3}\phi^{a_2}_{i,x_2}\phi^{a_3}_{i,x_3} + iG^{a_2a_3}_{ii,x_2x_3}\right)\phi^{a_4}_{i,x_4}$$
$$+\frac{1}{6}g^{a_1a_2a_3a_4}_{x_1x_2x_3x_4}g^{a_5a_6a_7a_8}_{x_5x_6x_7x_8}\sum_j G^{a_2a_5}_{ij,x_2x_5}G^{a_3a_6}_{ij,x_3x_6}G^{a_4a_7}_{ij,x_4x_7}\phi^{a_8}_{j,x_8}, \tag{57}$$

and

$$\delta_{ij}\delta_{x_1x_2}\delta^{a_1a_2} = \sum_k\left\{-\left[g_0^{-1}\right]^{a_1a_3}_{ik,x_1x_3} + \frac{1}{2}\delta_{ik}g^{a_1a_3a_4a_5}_{x_1x_3x_4x_5}\left(\phi^{a_4}_{i,x_4}\phi^{a_5}_{i,x_5} + iG^{a_4a_5}_{ii,x_4x_5}\right)\right\}G^{a_3a_2}_{kj,x_3x_2}$$
$$-\frac{i}{2}g^{a_1a_4a_5a_6}_{x_1x_4x_5x_6}g^{a_3a_7a_8a_9}_{x_3x_7x_8x_9}\sum_k G^{a_4a_7}_{ik,x_4x_7}G^{a_5a_8}_{ik,x_5x_8}\left(\phi^{a_6}_{i,x_6}\phi^{a_9}_{k,x_9} + \frac{i}{3}G^{a_6a_9}_{ik,x_6x_9}\right)G^{a_3a_2}_{kj,x_3x_2}. \tag{58}$$

These equations are one of our main results. In the form shown here they are not particularly amenable to solution, and we now discuss simplifications that allow us to obtain equations of motion that are easier to solve.

A. Low-frequency approximation

Equations (57) and (58), whilst having a compact form in our notation, contain as many as seven time integrals, making it very computationally expensive to solve the equations numerically. This suggests that some level of approximation is required in order to obtain more physical insight from the equations above. We assume that the sweep across the quantum critical region is not too fast and focus on the low frequency components of the equations of motion, making use of a similar approach to Ref. [30].

We first note that the components of $\left[\mathcal{G}^{-1}\right]^{a_1a_2}_{\alpha_1\alpha_2}(t_1,t_2)$ are time translation invariant [Eq. (28)] so that they depend on a single frequency. Provided we consider values of the chemical potential away from the degeneracy points between adjacent Mott lobes, i.e. $\mu \not\approx Ur$, with r an integer, then only $\left[\mathcal{G}^{-1}\right]^{a_1a_2}_{cq}(t_1,t_2)$ and $\left[\mathcal{G}^{-1}\right]^{a_1a_2}_{qc}(t_1,t_2)$ contribute, since $\left[\mathcal{G}^{-1}\right]^{a_1a_2}_{qq}(t_1,t_2)$ does not contribute to the low-frequency dynamics for $\mu \not\approx Ur$ [30]. We expand the Fourier transform of the inverse retarded Green's function:

$$\left[\mathcal{G}^R\right]^{-1}(\omega) \simeq \upsilon + \lambda\omega + \kappa^2\omega^2 + \ldots,$$

where

$$\upsilon = \left[\mathcal{G}^R\right]^{-1}(\omega=0), \tag{59}$$
$$\lambda = \frac{\partial}{\partial\omega}\left[\mathcal{G}^R\right]^{-1}(\omega)\Big|_{\omega=0}, \tag{60}$$
$$\kappa^2 = \frac{1}{2}\frac{\partial^2}{\partial\omega^2}\left[\mathcal{G}^R\right]^{-1}(\omega)\Big|_{\omega=0}. \tag{61}$$

The explicit expressions for υ, λ, and κ^2 are given in Appendix B. Applying the above approximations gives

$$\left[g_0^{-1}\right]^{a_1a_2}_{x_1x_2} \approx -\delta(t_1-t_2)\left[2\tau^1_{\alpha_1\alpha_2}\sigma_1^{a_1a_2}J_{ij}(t_1) + \delta_{ij}\mathcal{D}^{a_1a_2}_{\alpha_1\alpha_2}(t_1)\right], \tag{62}$$

with

$$\mathcal{D}^{a_1a_2}_{\alpha_1\alpha_2}(t_1) = \tau^1_{\alpha_1\alpha_2}\left[\sigma_1^{a_1a_2}\left(\upsilon - \kappa^2\partial^2_{t_1}\right) + \sigma_2^{a_1a_2}\lambda\partial_{t_1}\right]. \tag{63}$$

We also apply a low frequency approximation to the four-point vertex, $g^{(4)}$, which we can express as follows:

$$g^{a_1a_2a_3a_4}_{x_1x_2x_3x_4} = -u_1\delta(t_1-t_2)\delta(t_1-t_3)\delta(t_1-t_4)\zeta^{a_1a_2a_3a_4}_{x_1x_2x_3x_4} - u_2\left[\delta(t_1-t_2)\delta(t_3-t_4)\eta^{a_1a_2a_3a_4}_{x_1x_2x_3x_4} + \{2\leftrightarrow 3\} + \{2\leftrightarrow 4\}\right], \tag{64}$$

where u_1 and u_2 are defined in Appendix B and

$$\zeta^{a_1a_2a_3a_4}_{x_1x_2x_3x_4} \equiv \frac{1}{2}\left(\delta_{\alpha_1\alpha_2}\tau^1_{\alpha_3\alpha_4} + \tau^1_{\alpha_1\alpha_2}\delta_{\alpha_3\alpha_4}\right)$$
$$\times\left(\sigma_1^{a_1a_2}\sigma_1^{a_3a_4} + \sigma_1^{a_1a_3}\sigma_1^{a_2a_4} + \sigma_1^{a_1a_4}\sigma_1^{a_2a_3}\right), \tag{65}$$
$$\eta^{a_1a_2a_3a_4}_{x_1x_2x_3x_4} \equiv \tau^1_{\alpha_1\alpha_2}\tau^1_{\alpha_3\alpha_4}\sigma_1^{a_1a_2}\sigma_1^{a_3a_4}. \tag{66}$$

Terms in Eqs. (57) and (58) that are first-order in $g^{(4)}$ contain three time-integrals and those that are second-order in $g^{(4)}$ contain seven time-integrals. Applying the low-frequency approximation reduces the number of time integrals to at most one for first order terms and at most three for second order terms.

After the low-frequency approximation, we can orga-

nize the terms in the equations of motion as follows: terms proportional to u_1 contain no time integrals, terms proportional to u_1^2 or u_2 contain one time integral, and terms proportional to u_2^2 or u_1u_2 contain two or more time integrals. Numerical evaluation of u_1 and u_2, shown in Fig. 4 demonstrates that unless μ/U is close to an integer, the u_1 terms will dominate the u_2 terms and so we only retain terms of order u_1, u_2 or u_1^2, which at most leads to one time integral in all of the terms we consider in the equations of motion.

Applying the approximations described above, the equations of motion simplify to

$$\begin{aligned}
0 = {} & \mathcal{D}^{a_1a_2}_{\alpha_1\alpha_2}(t)\phi^{a_2}_{i,\alpha_2}(t_1) + 2\sum_k J_{ik}(t_1)\phi^{\bar{a_1}}_{k,\bar{\alpha_1}}(t) - \frac{1}{2}u_1\zeta^{a_1a_2a_3a_4}_{\alpha_1\alpha_2\alpha_3\alpha_4}\left(\frac{1}{3}\phi^{a_2}_{i,\alpha_2}(t_1)\phi^{a_3}_{i,\alpha_3}(t_1) + iG^{a_2a_3}_{ii,\alpha_2\alpha_3}(t_1,t_1)\right)\phi^{a_4}_{i,\alpha_4}(t_1) \\
& -\frac{1}{2}u_2\eta^{a_1a_2a_3a_4}_{\alpha_1\alpha_2\alpha_3\alpha_4}\int_{-\infty}^{\infty}dt_2\left(2\left(\frac{1}{3}\phi^{a_2}_{i,\alpha_2}(t_1)\phi^{a_3}_{i,\alpha_3}(t_2) + iG^{a_2a_3}_{ii,\alpha_2\alpha_3}(t_1,t_2)\right)\phi^{a_4}_{i,\alpha_4}(t_2)\right. \\
& \qquad \left. + \left(\frac{1}{3}\phi^{a_3}_{i,\alpha_3}(t_2)\phi^{a_4}_{i,\alpha_4}(t_2) + iG^{a_3a_4}_{ii,\alpha_3\alpha_4}(t_2,t_2)\right)\phi^{a_2}_{i,\alpha_2}(t_1)\right) \\
& +\frac{1}{6}u_1^2\zeta^{a_1a_2a_3a_4}_{\alpha_1\alpha_2\alpha_3\alpha_4}\zeta^{a_5a_6a_7a_8}_{\alpha_5\alpha_6\alpha_7\alpha_8}\sum_k\int_{-\infty}^{\infty}dt_2 G^{a_2a_5}_{ik,\alpha_2\alpha_5}(t_1,t_2)G^{a_3a_6}_{ik,\alpha_3\alpha_6}(t_1,t_2)G^{a_4a_7}_{ik,\alpha_4\alpha_7}(t_1,t_2)\phi^{a_8}_{k,\alpha_8}(t_2),
\end{aligned} \tag{67}$$

$$\begin{aligned}
\delta_{ij}\delta_{\alpha_1\alpha_2}\delta_{a_1a_2}\delta(t_1-t_2) = {} & \mathcal{D}^{a_1a_3}_{\alpha_1\alpha_3}(t_1)G^{a_3a_2}_{ij,\alpha_3\alpha_2}(t_1,t_2) + 2\sum_k J_{ik}(t_1)G^{\bar{a_1}a_2}_{kj,\bar{\alpha_1}\alpha_2}(t_1,t_2) \\
& -\frac{1}{2}u_1\zeta^{a_1a_3a_4a_5}_{\alpha_1\alpha_3\alpha_4\alpha_5}\left(\phi^{a_4}_{i,\alpha_4}(t_1)\phi^{a_5}_{i,\alpha_5}(t_1) + iG^{a_4a_5}_{ii,\alpha_4\alpha_5}(t_1,t_1)\right)G^{a_3a_2}_{ij,\alpha_3\alpha_2}(t_1,t_2) \\
& -\frac{1}{2}u_2\eta^{a_1a_3a_4a_5}_{\alpha_1\alpha_3\alpha_4\alpha_5}\int_{-\infty}^{\infty}dt_3\left[\phi^{a_4}_{i,\alpha_4}(t_3)\phi^{a_5}_{i,\alpha_5}(t_3) + iG^{a_4a_5}_{ii,\alpha_4\alpha_5}(t_3,t_3)\right]G^{a_3a_2}_{ij,\alpha_3\alpha_2}(t_1,t_2) \\
& -u_2\eta^{a_1a_4a_3a_5}_{\alpha_1\alpha_4\alpha_3\alpha_5}\int_{-\infty}^{\infty}dt_3\left[\phi^{a_4}_{i,\alpha_4}(t_1)\phi^{a_5}_{i,\alpha_5}(t_3) + iG^{a_4a_5}_{ii,\alpha_4\alpha_5}(t_1,t_3)\right]G^{a_3a_2}_{ij,\alpha_3\alpha_2}(t_3,t_2) \\
& -\frac{i}{2}u_1^2\zeta^{a_1a_4a_5a_6}_{\alpha_1\alpha_4\alpha_5\alpha_6}\zeta^{a_3a_7a_8a_9}_{\alpha_3\alpha_7\alpha_8\alpha_9}\sum_k\int_{-\infty}^{\infty}dt_3 G^{a_4a_7}_{ik,\alpha_4\alpha_7}(t_1,t_3)G^{a_5a_8}_{ik,\alpha_5\alpha_8}(t_1,t_3) \\
& \qquad \times\left(\phi^{a_6}_{i,\alpha_6}(t_1)\phi^{a_9}_{k,\alpha_9}(t_3) + \frac{i}{3}G^{a_6a_9}_{ik,\alpha_6\alpha_9}(t_1,t_3)\right)G^{a_3a_2}_{kj,\alpha_3\alpha_2}(t_3,t_2),
\end{aligned} \tag{68}$$

a system of second-order nonlinear integro-differential equations with single time-integrals only.

Equations of motion for the Bose Hubbard model were previously derived within a two particle irreducible formalism by Rey *et al.* [70] for weak interactions. We emphasise that Eqs. (67) and (68) allow one to consider strong as well as weak interactions. The structure of the equations is similar, but there are some important differences – in Ref. [70] the equations of motion only have first order derivatives in time, while the equations of motion considered here also contain second order time derivatives. Another important difference is that here non-local effects in time occur at first order in the interaction vertices $g^{(4)}$ (due to the presence of the u_2 terms), in contrast with Ref. [70] where nonlocality arises at second order in the interaction vertices.

B. Keldysh structure of G

Before presenting numerical results, it is worth discussing the explicit Keldysh structure of the full propagator G and the mean field ϕ. Following Refs. [70, 82], we can express G as follows

$$G^{a_1a_2}_{ij,qq}(t_1,t_2) = 0, \tag{69}$$

$$G^{a_1a_2}_{ij,qc}(t_1,t_2) = i\theta(t_2-t_1)G^{a_1a_2,(\rho)}_{ij}(t_1,t_2), \tag{70}$$

$$G^{a_1a_2}_{ij,cq}(t_1,t_2) = -i\theta(t_1-t_2)G^{a_1a_2,(\rho)}_{ij}(t_1,t_2), \tag{71}$$

$$G^{a_1a_2}_{ij,cc}(t_1,t_2) = 2G^{a_1a_2,(F)}_{ij}(t_1,t_2), \tag{72}$$

with

$$G^{a_1a_2,(\rho)}_{ij}(t_1,t_2) \equiv i\langle\hat{a}^{a_1}_i(t_1)\hat{a}^{a_2}_j(t_2) - \hat{a}^{a_2}_j(t_2)\hat{a}^{a_1}_i(t_1)\rangle, \tag{73}$$

$$G^{a_1a_2,(F)}_{ij}(t_1,t_2) \equiv -\frac{i}{2}\langle\hat{a}^{a_1}_i(t_1)\hat{a}^{a_2}_j(t_2) + \hat{a}^{a_2}_j(t_2)\hat{a}^{a_1}_i(t_1)\rangle, \tag{74}$$

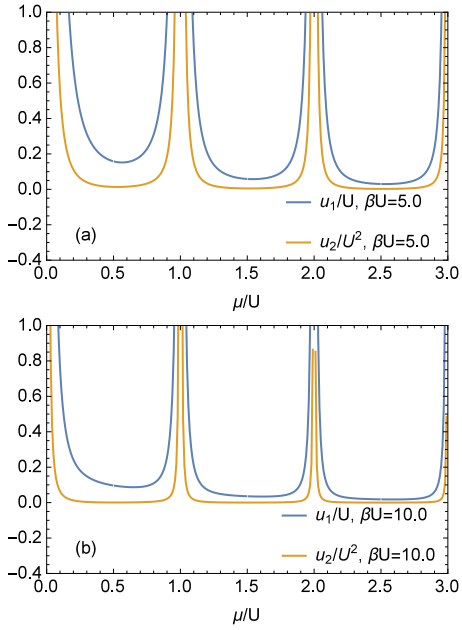

FIG. 4. (Color online) (a) Plot of u_1 and u_2 as a function of μ/U for inverse temperature $\beta U = 5.0$; and (b) for $\beta U = 10.0$.

where $G^{(\rho)}$ is usually called the spectral function and $G^{(F)}$ the statistical propagator [83]. One can then proceed to define the normal ρ, and anomalous, m, spectral and statistical functions [70]:

$$\rho_{ij}^{(\rho,F)}(t_1,t_2) \equiv G_{ij}^{21,(\rho,F)}(t_1,t_2), \tag{75}$$

$$m_{ij}^{(\rho,F)}(t_1,t_2) \equiv G_{ij}^{11,(\rho,F)}(t_1,t_2). \tag{76}$$

The m-functions are anomalous in the sense that they are only non-zero if the system is in a broken symmetry state (e.g. the superfluid state).

The mean field ϕ has the following Keldysh structure [65]

$$\begin{pmatrix} \phi_{i,q}^a(t) \\ \phi_{i,c}^a(t) \end{pmatrix} = \begin{pmatrix} 0 \\ \sqrt{2}\phi_i^a(t) \end{pmatrix}, \tag{77}$$

where $\phi_i^a(t)$ is the superfluid order parameter.

One can now express the equations of motion in terms of the superfluid order parameter and the four independent correlation functions $\rho^{(\rho,F)}$ and $m^{(\rho,F)}$. The equations of motion obtained by Rey *et al.* (see Appendix B of Ref. [70]) may also be obtained by setting

$$\upsilon \to 0, \lambda \to 1, \kappa^2 \to 0, u_1 \to -U, u_2 \to 0, \tag{78}$$

$$\rho^{(\rho,F)} \to -i\rho^{(\rho,F)}, m^{(\rho,F)} \to -im^{(\rho,F)}. \tag{79}$$

The last line reflects that our definition of G differs from that found in Ref. [70] by a factor of i.

IV. NUMERICAL RESULTS

Even after taking the low frequency approximation to simplify the equations of motion Eqs. (67) and (68), they are non-linear integro-differential equations, hence we take a numerical approach to solve them. This presents more of a challenge than the 1PI equations of motion obtained in Ref. [30], due to the presence of memory kernels that incorporate the entire history of the system, making explicit the importance of the quench protocol to the post-quench state. An additional important feature of the equations of motion is that they are causal, i.e. all quantities at some later time t_f can be obtained by integration over the known functions for times $t \leq t_f$. We exploit this feature of the equations to develop a finite-difference scheme to integrate them numerically. We have found that for quenches in which both the initial and final parameters correspond to the Mott phase, we can solve the equations of motion using an explicit finite difference scheme. For more general quenches, which also involve the superfluid phase, we have found that the equations become stiff and explicit methods become unstable, necessitating the use of implicit methods. Due to the combination of numerical stability and memory requirements we only present results for quenches in the Mott phase, and defer numerical results for quenches from the superfluid to Mott phase to future work. In this section, we first discuss the details of our numerical scheme, and then pay careful attention to the initial conditions, assuming that we are starting from an equilibrium state. We then present numerical results for the quasi-momentum distribution for quenches in the Mott phase and of light-cone like propagation of correlations in one and two dimensions.

A. Numerical Algorithm

To solve Eqs. (67) and (68) numerically, we discretize time, so that times t and t' are represented by integers n and m via $t = n\Delta t$ and $t' = m\Delta t$, where Δt is the timestep. Given that we are working on a lattice, space is already discretized. We approximate time derivatives using a second-order central difference scheme [82], e.g. for a function $f_{ij}(t,t')$ evaluated at lattice sites i and j at times t and t':

$$\partial_t f_{ij}(t,t') \mapsto \frac{1}{2\Delta t}\left(f_{ij,n+1m} - f_{ij,n-1m}\right), \tag{80}$$

$$\partial_t^2 f_{ij}(t,t') \mapsto \frac{1}{\Delta t^2}\left(f_{ij,n+1m} - 2f_{ij,nm} + f_{ij,n-1m}\right), \tag{81}$$

where

$$f_{ij,nm} = f_{ij}(n\Delta t, m\Delta t).$$

We evaluate integrals using the trapezoidal rule, e.g.

$$\int_{-\infty}^{t} dt_1 f_{ij}(t_1,t') \mapsto \sum_{l=0}^{n} f_{ij,lm}, \tag{82}$$

which is also accurate to second-order in the timestep. The discretized equations of motion for $\phi_{i,n}$ and the matrices $(\rho,m)^{(\rho,F)}_{ij,nm}$ have two features that make them amenable to numerical solution, i) for fixed m, the equations advance in the n direction [70, 82], and ii) due to symmetry, only half of the (n,m)-matrix elements have to be computed and stored in memory. Furthermore, due to the bosonic commutation relations, the diagonal elements $\rho^{(\rho)}_{ij,nn} = -\delta_{ij}, m^{(\rho)}_{ij,nn} = 0$ are fixed for all n. The discretized system of equations can be solved explicitly: starting with $n = 1$, for the time step $n+1$ one computes successively all entries with $m = 0,\ldots,n+1$ from known functions evaluated at earlier times [70, 82]. This requires one to specify the following initial conditions: $\phi_{i,0}$, $\phi_{i,1}$, $(\rho,m)^{(F)}_{ij,00}$, $(\rho,m)^{(F)}_{ij,10}$, $(\rho,m)^{(F)}_{ij,11}$, and $(\rho,m)^{(\rho)}_{ij,10}$, which we discuss in Sec. IV B.

The main computational constraint on the algorithm comes from the time integrals, which require considerable processing and memory resources. For homogeneous systems, if N_s is the number of sites, and N_t is the number of timesteps then the memory requirements scale like $\frac{1}{2}N_sN_t^2$. Previous nonequilibrium 2PI studies which integrated similar equations of motion did not keep all of the history of the memory kernels for large times, which was justified by the argument that the two-time correlator would damp at an exponential rate [70, 82]. We do not make this assumption since it does not always hold for the quench protocols we consider and choose Δt to be sufficiently small such that the results we obtain are independent of the choice of timestep.

B. Initial conditions

As noted in Sec. IV A the equations of motion require initial conditions to be specified for several different quantities. The equations of motion Eqs. (67) and (68) are appproximate due to taking the low frequency limit, so if we start from equilibrium initial conditions for the BHM and then quench, then the subsequent dynamics will have contributions from the relaxation of the BHM equilibrium to the equilibrium for the equations of motion (which will differ slightly from the equilibrium for the full BHM due to taking the low frequency approximation) as well as from the quench itself. To address this issue, we take a two-step approach to solving the equations of motion numerically. We first start with initial conditions for the BHM that do not include a low frequency approximation and then evolve them keeping the parameters in the BHM constant using Eqs. (67) and (68) until the state is stationary. We then treat this stationary state as the equilibrium initial state and then begin the quench. By separating the calculations in this way, our goal is to isolate the instrinsic dynamics associated with the quench from extrinsic effects that are a result of the low frequency approximation. We discuss the details of this approach below.

We now specify exactly how we obtain the stationary state. Considering only terms to zero-loop order in Eq. (50) and to one-loop order in Eq. (51), one can obtain an analytical equilibrium solution to these equations of motion. This corresponds to keeping only the first term on the left-hand-side (LHS) of Eq. (50) and dropping the 2PI self-energy term on the right-hand-side (RHS) of Eq. (51). This is equivalent to a mean-field approximation of the order parameter ϕ and a Bogoliubov approximation of the Green's functions G. Furthermore, in order to obtain properly normalized spectral Green's functions, we do not apply any low-frequency approximation to the inverse bare propagator g_0^{-1}, however we approximate the interaction vertex u by its static limit. In Appendix C, we give details of this calculation. Our analytical equilibrium solution is in agreement with the equilibrium solution obtained via the imaginary-time formalism by Sengupta and Dupuis in Ref. [59].

To relax the system from the initial state described above to a stationary state, we evolve the system by simultaneously solving the approximate equations of motion Eqs. (67) and (68) using the numerical algorithm described in Sec. IV A. In an equilibrium state, single-time quantities should be time-independent, e.g. $\phi(t) = \phi$, and two-time quantities should only depend on their time differences, e.g. $G(t,t') = G(t-t')$. One way to check this is by monitoring the quasi-momentum distribution $n_{\mathbf{k}}(t)$

$$n_{\mathbf{k}}(t) = \frac{1}{N_s}\sum_{i,j} e^{-i\mathbf{k}\cdot(\mathbf{r}_i-\mathbf{r}_j)} \times \left(\phi_i(t)\phi_j(t) + i\rho^{(F)}_{ij}(t,t) - \frac{1}{2}\delta_{ij}\right), \tag{83}$$

where N_s is the total number of lattice sites and $\mathbf{r}_i$ and $\mathbf{r}_j$ are the locations of site i and site j respectively. A plot of $n_{\mathbf{k}}(t)$ as a function of t shows oscillations inside an envelope that decays exponentially to a constant value. In Fig. 5, we plot the relaxation of $n_{\mathbf{k}}(t)$ for a $N_s = 36$ site square (6×6) system.

The initial relaxation segment of our numerical runs is similar to the out-of-equilibrium scenarios considered in Refs. [70, 82]. In each of these cases, the system starts in an out-of-equilibrium state and is then allowed to relax. A difference in the case considered here is that our initial state should be quite close to the stationary state to which the system relaxes. As a result, similarly to Refs. [70, 82], it is not necessary to keep all the history of the memory kernels during the relaxation period. To be more specific, there exists a time window of length t_W such that for $t > t_W$ one can approximate the integrals found in the equations of motion [see Eqs. (D6) and (D7)]

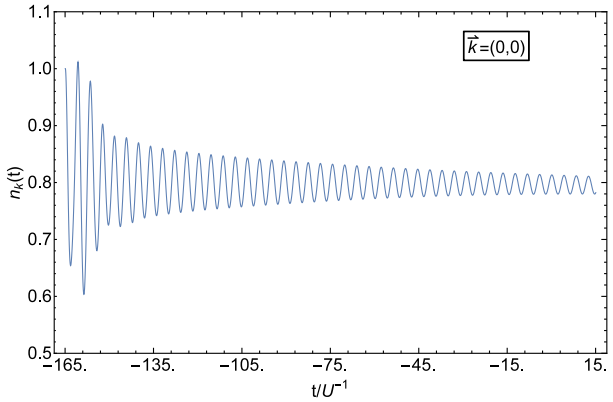

FIG. 5. (Color online) Plot of $n_{\mathbf{k}}(t)$ during initial relaxation period for $\mathbf{k} = 0$, $\mu/U = 0.25$, $T = 0$, $N_s = 36$, $d = 2$.

as follows

$$\int_{-\infty}^{t} dt_1 \approx \int_{t-t_W}^{t} dt_1, \tag{84}$$

$$\int_{t'}^{t} dt_1 \approx \int_{t-t_W}^{t} dt_1, \tag{85}$$

where Eq. (85) holds as long as $t_W < t - t'$. Only when the quench begins do we need to retain all of the subsequent history of the system.

C. MI quenches

We consider quenches in which the hopping parameter $J_{ij}(t)$ is tuned as a function of time. [Experimentally this corresponds to the scenario in which the depth of the optical lattice is varied, since hopping varies exponentially with lattice depth while interactions vary weakly with lattice depth [84].] We assume that hopping is only between nearest neighbour sites on a d-dimensional hypercubic lattice:

$$J_{ij}(t) = \begin{cases} \frac{1}{2z}\left(-\upsilon - \delta(t)\right) & \text{for nearest neighbours} \\ 0 & \text{otherwise} \end{cases}, \tag{86}$$

where $z = 2d$ is the coordination number and noting that $\upsilon = -\frac{1}{z}J_0$, where J_0 is the value of the hopping at the mean field phase boundary. We choose $\delta(t)$ to have the form:

$$\delta(t) = \left(\frac{\delta_0 + \delta_1}{2}\right)\tanh\left(\frac{t}{\tau_Q}\right) + \left(\frac{\delta_1 - \delta_0}{2}\right). \tag{87}$$

Note that $\lim_{t\to-\infty}\delta(t) = -\delta_0$, and $\lim_{t\to\infty}\delta(t) = \delta_1$. The time scale τ_Q is the characteristic time for $\delta(t)$ to cross from $-\delta_0$ to δ_1. $\delta(t)$ is a smooth function that is linear in the vicinity of $t = 0$, corresponding to the experimental scenario of a linear ramp. Other forms of $\delta(t)$ which are not linear may lead to differing behaviour in the long-time limit [85]. For a quench from superfluid to Mott insulator, $\delta_0, \delta_1 > 0$, but for the quenches within the Mott insulator we consider here, $\delta_0 < 0, \delta_1 > 0$.

Using the numerical algorithm discussed in Sec. IV A, the initialization discussed in Sec. IV B along with the quench protocol shown in Eq. (87) we integrated the equations of motion for quenches in which both the initial and final values of hopping correspond to insulating states at equilibrium. The numerical simulations are simpler for this type of quench for two reasons: i) if the system is not in the superfluid phase we can ignore the symmetry-breaking terms of the equations of motion, and ii) less computational resources are required in order to obtain stable numerical results, as discussed at the beginning of Sec. IV. To be more precise on point i), in the MI regime, the order parameter ϕ and the anomalous Green's functions $m^{(\rho,F)}$ vanish, simplifying the equations of motion. We display the explicit form of the equations of motion when these terms vanish in Appendix D.

In Fig. 6 we show the quasi-momentum distribution $n_{\mathbf{k}}(t)$ calculated for all independent k vectors as a function of time during a quench for a) an 18 site chain and b) a 36 site square system. In both cases, $\mu/U = 0.25$ and $\beta U = \infty$. In panel c) we show the quasi-momentum distribution at $\mathbf{k} = 0$ for the 6×6 system for a variety of quench timescales τ_Q – for the quenches we consider, the long time limit is the same in all cases, and we have verified that if we rescale time with τ_Q then the curves essentially collapse on each other. We have also checked the system size dependence of our results, and find that in two dimensions, the curves are essentially independent of N_s, the number of sites. We believe this is because we are studying quenches within the MI regime where the correlation length is very short. We notice that in both the one and two dimensional cases, the quasi-momentum distribution grows more at $\mathbf{k} = 0$ than any other wavevector as J/U increases, and in fact there is a small amount of depletion from higher-momentum states after the quench. Together, these results are consistent with a growing correlation length as the superfluid phase is approached, in qualitative agreement with both numerical [57] and experimental [8] quench studies.

D. Light-cone spreading of correlations

In addition to focusing on the dynamics of correlations in momentum space, we also investigated the time evolution of correlations in real space for a quench in the MI regime, and found light-cone like spreading [44] of these correlations in one and two dimensions. We compare the velocities we obtain for the propagation of correlations to existing results in the field [41, 45–49].

In Fig. 7(a) we display the time evolution of the single-particle correlation function $\rho^{(F)}_{\Delta x}(t,t)$ at equal-times for the same 18-site chain considered in Fig. 6(a) (the only difference being the choice that $\tau_Q = 5$ rather than

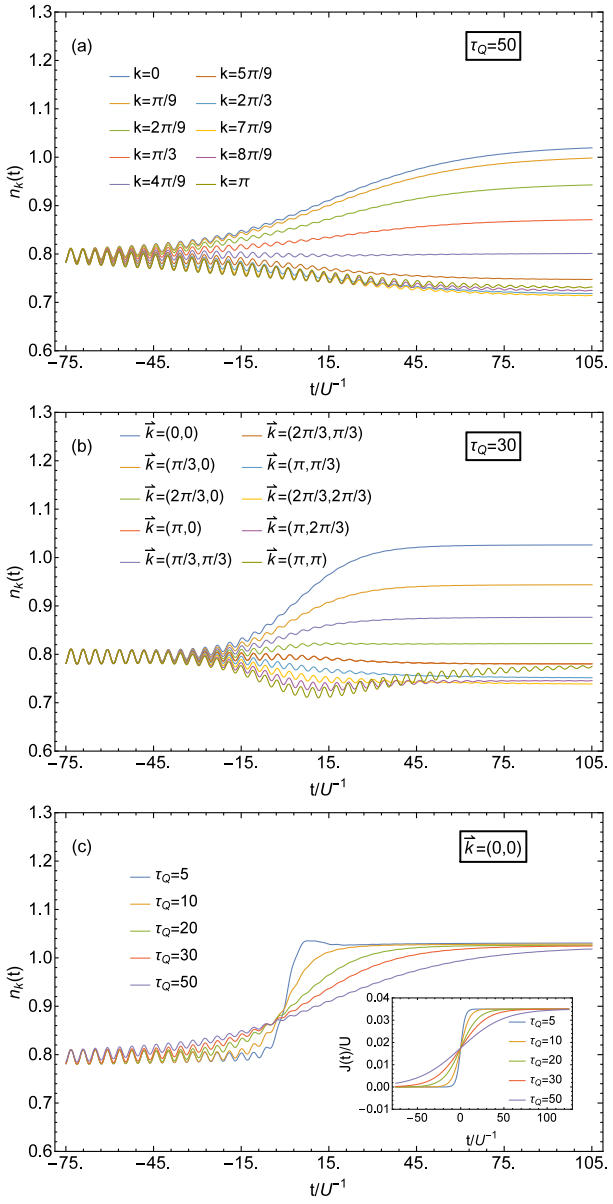

FIG. 6. (Color online) Dynamics of $n_{\mathbf{k}}(t)$: (a) plotted for a variety of $\mathbf{k}$ at fixed $\tau_Q = 50$ for $N_s = 18$ and $d = 1$, (b) plotted for a variety of $\mathbf{k}$ at fixed $\tau_Q = 30$ for $N_s = 36$ and $d = 2$, (c) plotted for a variety of τ_Q at fixed $\mathbf{k} = (0, 0)$ for $N_s = 36$ and $d = 2$. In each case the remaining parameters are $\beta U = \infty$, $\mu/U = 0.25$, $\lambda = -0.28$, $\kappa^2 = 1.024$, $u_1 = 1.277$, $u_2 = 0$, and the hopping parameters are $\delta_0 = -0.15$, $\delta_1 = 0.01$. The inset in panel (c) shows the value of J/U during each quench run.

$\tau_Q = 50$), where each curve corresponds to a different separation distance Δx. From this figure, we can see the emergence of correlation wave-packets after the quench. Moreover, zooming-in on this plot [Fig. 7(b)] one can see the propagation of the wave-packet along the 1D chain. We use the data shown in Fig. 7(a) and (b) to find the time at which the wavepacket has maximum amplitude for a given Δx and in Fig. 7(c) we plot the lattice position $\Delta x/a$ of the wave-packet against time t/U^{-1}.

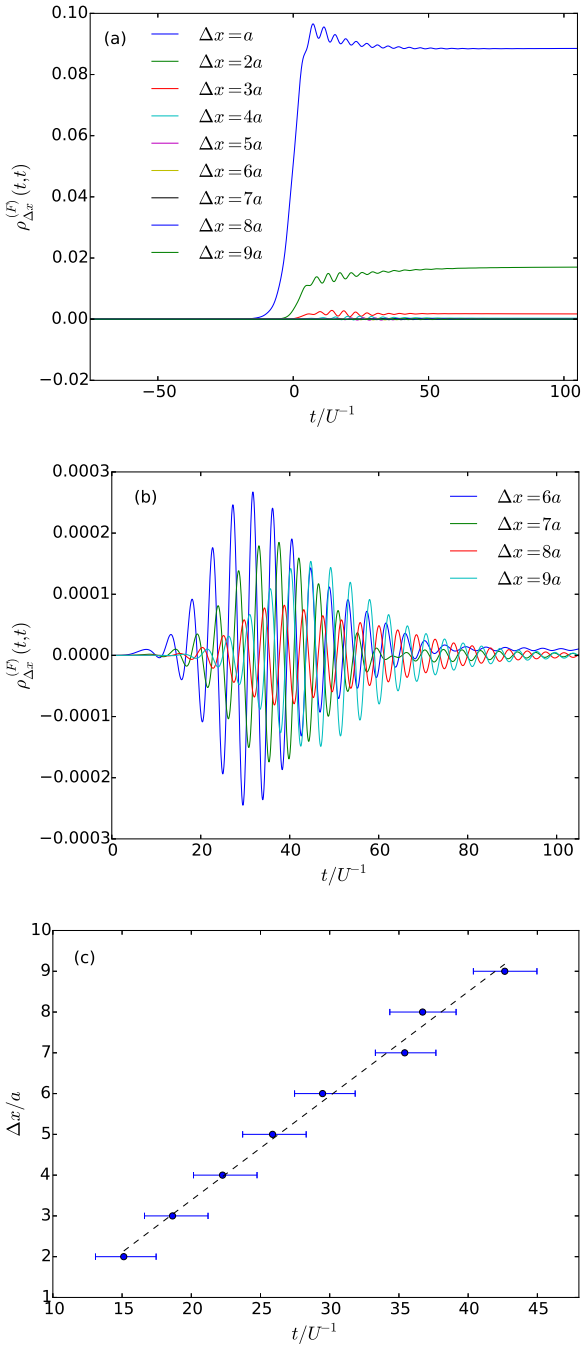

FIG. 7. (Color online) (a) Dynamics of $\rho^{(F)}_{\Delta x}(t, t)$ for $\Delta x \neq 0$, (b) zoom-in of plot (a), (c) scatter plot of the time t/U^{-1} it takes for the single-particle correlation front to travel a distance Δx. We show a straight line fit to the data. The parameters for (a)-(c) are $\beta U = \infty$, $\mu/U = 0.25$, $\lambda = -0.28$, $\kappa^2 = 1.024$, $u_1 = 1.277$, $u_2 = 0$, $\delta_0 = -0.15$, $\delta_1 = 0.01$, $N_s = 18$, and $d = 1$.

The data shown in Fig. 7(c) is compatible with a linear fit, implying that there is a propagating front of single-

particle correlations that travels through the 1D chain at a constant velocity v_{1D}. Performing a linear fit we obtain an estimate for the velocity of

$$v_{1D} \simeq 3.7\frac{Ja}{\hbar}.$$

This value is similar in magnitude, but slightly less than values obtained by Barmettler *et al.* using a fermionization procedure in one dimension [46]. These values are $v_{1D} = 6Ja/\hbar$ for $\bar{n} = 1$ in the limit of infinitely strong interactions and $v_{1D} = 4Ja/\hbar$ in the limit of no interactions. Recent calculations of correlations in one dimension for weak interactions also found a value of $v_{1D} = 3.7Ja/\hbar$ [49].

We performed similar calculations of the spreading of correlations in two dimensional systems as well as one dimension, and found a similar light-cone like spreading of correlations as shown in Fig. 8(a) for a 64 site square (8×8) system with the same parameters as those in the 18 site chain above except that $\delta_1 = 0.001$. From Fig. 8(a) we are again able to obtain an estimate of the velocity for the spreading of correlations:

$$v_{2D} \simeq 2.9\frac{Ja}{\hbar}.$$

There has been one estimate for the speed of spreading of correlations in the BHM in dimensions higher than one that we are aware of: Navez and Schützhold [48] performed an expansion in inverse co-ordination number about mean field theory, which for the parameters we used here would give $v_{2D} \simeq 6.2Ja/\hbar$. Unlike our result, in which we find correlations spread slightly more slowly in two dimensions than one dimension, Ref. [48] suggests that they spread more quickly than one dimension in higher dimensions. Given that our approach can be expected to be more accurate with increasing dimensionality and is already quite close to results obtained from other methods in one dimension, we believe that our result is likely to be reasonably close to the exact value of v_{2D}.

Lastly, we consider the decay of long-time single-particle correlations $\rho^{(F)}_{\Delta r}(t_f, t_f)$ in space as a function of Δr. In Fig. 8(b) we plot $\rho^{(F)}_{\Delta r}(t_f, t_f)$ against Δr for $\mu/U = 0.25$, $\beta U = \infty$, $\delta_0 = -0.15$, $\delta_1 = 0.01$, $\tau_Q = 5$, $N_s = 36$, and $d = 2$. To extract an estimate for the correlation length ξ, we fit the correlation function to

$$\rho^{(F)}_{\Delta r}(t_f, t_f) = \rho^{(F)}_0(t_f, t_f)e^{-|\Delta r|/\xi}.$$

The inset to Fig. 8(b) shows the value of ξ as a function of the final hopping value $(J/U)_f$ where we see that the correlation length depends linearly on the final hopping and grows with increasing $(J/U)_f$ as we would expect as the superfluid phase is approached.

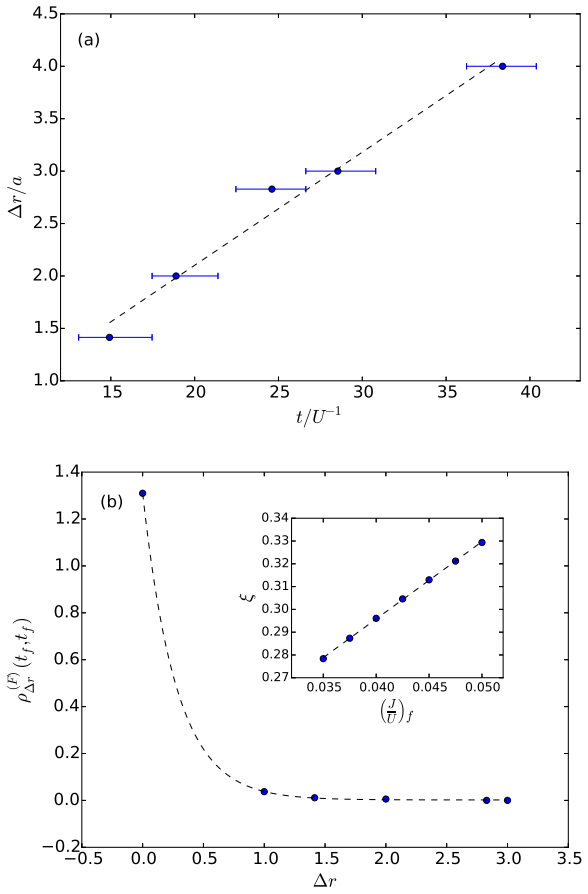

FIG. 8. (Color online) (a) Scatter plot of the time t/U^{-1} it takes for the single-particle correlation front to travel a distance Δr for a $N_s = 64$ site square (8×8) system, with a straight line fit to the data. (b) Plot of $\rho^{(F)}_{\Delta r}(t_f, t_f)$ as a function of Δr for $\delta_1 = 0.01$, fitted to $\rho^{(F)}_0(t_f, t_f)e^{-|\Delta r|/\xi}$ with $\xi = 0.278$. The inset of panel (b) plots ξ as a function of $\left(\frac{J}{U}\right)_f$. The remaining parameters for both (a) and (b) are $\beta U = \infty$, $\mu/U = 0.25$.

V. DISCUSSION AND CONCLUSIONS

The ability to address single sites in cold atom experiments has allowed for experimental exploration of spatio-temporal correlations in the BHM [47]. This has led to theoretical investigations of the space and time dependence of these correlations in both one [46] and higher dimensions [49, 57] in the presence of a quench. In dimensions higher than one, where numerical approaches are limited, a theoretical challenge has been to develop a framework which can treat correlations in both the superfluid and Mott insulating phases over the course of a quench. An important result in this paper is that we have developed a formalism that allows for the description of the space and time dependence of correlations in both phases during a quench. The specific approach we took was to derive a 2PI effective action for the BHM us-

ing the Schwinger-Keldysh technique building on the 1PI real-time strong-coupling theory developed in Ref. [30] which generalized the imaginary-time theory developed in Ref. [59]. From this 2PI effective action we were able to derive equations of motion that treat the superfluid order parameter and the full two-point Green's functions on equal footing. We emphasise that our formalism is applicable even in the limit of low occupation number per site.

Even at the level of the 1PI real-time theory, the quartic coupling becomes non-local in time, which in the 2PI theory to second order in the interaction vertices leads to complicated expressions in the equations of motion, involving up to seven time integrals. We showed that by taking a low frequency approximation, this complexity can be reduced to at most a single time integral. The equations of motion obtained at this point are somewhat similar to previous 2PI studies of the out of equilibrium dynamics of interacting bosons [70, 82]. However, in contrast to these previous studies, the equations of motion we obtain are second-order rather than first order in time and non-local effects in time appear at first order in the interaction vertices instead of at second order. We solved these equations for quenches in the Mott phase and studied the dynamics of the quasi-momentum distribution $n_{\mathbf{k}}(t)$, which show a growth in the peak at $\mathbf{k} = 0$.

From the calculation of the real-space spreading of single-particle correlations in one and two dimensions, we demonstrated light-cone like spreading of correlations. The velocity we obtain in one dimension, $v_{1D} \simeq 3.7Ja/\hbar$, is similar to recent theoretical [45, 46, 49] and experimental results [47] and gives confidence that the result we found in two dimensions, $v_{2D} \simeq 2.9Ja/\hbar$, is robust. In particular, the one dimensional result suggests that the approximations we made in only keeping certain diagrams in the 2PI effective action and the low frequency approximation still allow us to obtain much of the essential quench physics of the BHM. Our results indicate that the spreading of correlations in the Mott phase of the BHM is slower in two dimensions than in one by about 20%, which should potentially be a large enough effect to be verified experimentally in cold atom experiments.

The space and time dependence of correlations after a quantum quench give insight into the propagation of excitations generated by that quench, and hence we hope that the formalism we have developed here will allow further theoretical investigation of the excitations after quenches in the BHM, to complement experimental efforts in the same direction. In future work we plan to investigate a broader range of quench protocols, and generalizations such as the inclusion of a harmonic trap, coupling to a bath [66, 86] or multicomponent Bose Hubbard models.

VI. ACKNOWLEDGEMENTS

The authors thank N. Dupuis, T. Gasenzer and A. M. Rey for helpful communications. This work was supported by NSERC.

Appendix A: One particle irreducible (1PI) approach to the BHM

In this appendix, we briefly review the derivation of the 1PI action for the BHM and correct some minor mistakes in Ref. [30] (all of these mistakes relate to mislabelling of Keldysh indices – numerical results in Ref. [30] are unaffected). First introduce an auxiliary field ψ via a complex Hubbard-Stratonovich transformation [30] so the generating functional $\mathcal{Z}[f]$ takes the form (after Keldysh rotation)

$$\begin{aligned}\mathcal{Z}[f] = \int [\mathcal{D}\psi^*][\mathcal{D}\psi] \int [\mathcal{D}a^*][\mathcal{D}a] \\ \times e^{-\frac{i}{2}\int_{-\infty}^{\infty} dt \sum_{ij} \psi^*_{i\overline{\alpha}}(t)[J]^{-1}_{ij}\psi_{j\alpha}(t)} \\ \times e^{-iS_\psi[a]+iS_0[a]+iS_f[a]},\end{aligned} \tag{A1}$$

where S_0 is the BHM action in the local (i.e. $J_{ij} = 0$) limit

$$S_0 = \int_{-\infty}^{\infty} dt \sum_i [a^*_{i\overline{\alpha}}(t)(i\partial_t)a_{i\alpha}(t)] + S_U, \tag{A2}$$

and

$$S_\psi = \int_{-\infty}^{\infty} dt \sum_i \psi^{\overline{a}}_{i,\overline{\alpha}}(t) a^a_{i,\alpha}(t). \tag{A3}$$

We can eliminate the iS_f term in Eq. (A1) by shifting the field $\psi^a_{i\alpha}(t) \to \psi^a_{i\alpha}(t) + f^a_{i\alpha}(t)$ which gives

$$\begin{aligned}\mathcal{Z}[f] = \int [\mathcal{D}\psi^*][\mathcal{D}\psi] e^{iW_0[\psi]} \\ \times e^{-\frac{i}{2}\int_{-\infty}^{\infty} dt \sum_{ij} (\psi^*_{i\overline{\alpha}}(t)+f^*_{i\overline{\alpha}}(t))[J]^{-1}_{ij}(\psi_{j\alpha}(t)+f_{j\alpha}(t))},\end{aligned} \tag{A4}$$

where

$$e^{iW_0[\psi]} = \frac{1}{\mathcal{N}_0} \int [\mathcal{D}a^*][\mathcal{D}a] e^{iS_0[a]+iS_\psi}, \tag{A5}$$

$$\mathcal{N}_0 = \int [\mathcal{D}a^*][\mathcal{D}a] e^{iS_0[a]}. \tag{A6}$$

Comparing Eq. (A5) with Eq. (12), we see that $W_0[\psi]$ is the generator of local CCOGFs (which we will denote by $\mathcal{G}^{n,c}$) for the bosonic field a. The only non-vanishing local CCOGFs are those of the following form

$$\mathcal{G}^{n,c}_{i,\alpha_1,\ldots,\alpha_n,\alpha'_1,\ldots,\alpha'_n}(t_1,\ldots,t_n,t'_1,\ldots,t'_n) \equiv (-1)^n \left.\frac{\delta^{2n} W_0[\psi]}{\delta\psi^*_{i,\overline{\alpha}_1}(t_1)\ldots\delta\psi^*_{i,\overline{\alpha}_n}(t_n)\delta\psi_{i,\overline{\alpha}'_1}(t'_1)\ldots\delta\psi_{i,\overline{\alpha}'_n}(t'_n)}\right|_{\psi=0}$$
$$= i(-1)^n \left\langle a_{i,\alpha_1}(t_1)\ldots a_{i,\alpha_n}(t_n) a^*_{i,\alpha'_1}(t'_1)\ldots a^*_{i,\alpha'_n}(t'_n)\right\rangle^c_{S_0}, \tag{A7}$$

which are local to site i and have the same number of a and a^* fields. [Note that for the uniform BHM as considered here, the local CCOGF are independent of site index, and so we drop this index in the main text for the local CCOGF]. The superscript c indicates a connected function. Note that Eq. (A7) corrects Eq. (6) in Ref. [30]. These local CCOGFs satisfy the following symmetry property

$$\mathcal{G}^{n,c}_{i,\alpha_1,\ldots,\alpha_n,\alpha'_1,\ldots,\alpha'_n}(t_1,\ldots,t_n,t'_1,\ldots,t'_n) = \mathcal{G}^{n,c}_{i,\alpha_{p_1},\ldots,\alpha_{p_n},\alpha'_{p'_1},\ldots,\alpha'_{p'_n}}(t_{p_1},\ldots,t_{p_n},t'_{p'_1},\ldots,t'_{p'_n}). \tag{A8}$$

Inverting Eq. (A7), we may write (correcting Eqs. (7) and (8) in Ref. [30])

$$W_0[\psi] = -\sum_i \sum_{n=1}^{\infty} \frac{1}{(n!)^2} \int_{-\infty}^{\infty} \left[\prod_{l=1}^{n} dt_l dt'_l\right] \times \psi^*_{i,\overline{\alpha}_1}(t_1)\ldots\psi^*_{i,\overline{\alpha}_n}(t_n)\psi_{i,\overline{\alpha}'_1}(t'_1)\ldots\psi_{i,\overline{\alpha}'_n}(t'_n) \times \mathcal{G}^{n,c}_{i,\alpha_1,\ldots,\alpha_n,\alpha'_1,\ldots,\alpha'_n}(t_1,\ldots,t_n,t'_1,\ldots,t'_n), \tag{A9}$$

and so

$$e^{iW_0[\psi]} = e^{i\sum_{n=1}^{\infty} S^n_{\rm int}[\psi]}, \tag{A10}$$

where

$$S^n_{\rm int}[\psi] = -\frac{1}{(n!)^2}\sum_i \int_{-\infty}^{\infty} \left[\prod_{l=1}^{n} dt_l dt'_l\right] \times \psi^*_{i,\overline{\alpha}_1}(t_1)\ldots\psi^*_{i,\overline{\alpha}_n}(t_n)\psi_{i,\overline{\alpha}'_1}(t'_1)\ldots\psi_{i,\overline{\alpha}'_n}(t'_n) \times \mathcal{G}^{n,c}_{i,\alpha_1,\ldots,\alpha_n,\alpha'_1,\ldots,\alpha'_n}(t_1,\ldots,t_n,t'_1,\ldots,t'_n). \tag{A11}$$

Truncating $W_0[\psi]$ to quartic order in the ψ fields and setting the source currents f to zero in Eq. (A4), the action from Eq. (A4) is found to be

$$S_{\rm eff}[\psi] = -\frac{1}{2}\int_{-\infty}^{\infty} dt \sum_{ij} \psi^*_{i\overline{\alpha}}(t)\,[J]^{-1}_{ij}\,\psi_{j\alpha}(t) - \int_{-\infty}^{\infty} dt dt' \sum_i \psi^*_{i\overline{\alpha}}(t)\mathcal{G}^{1,c}_{i\alpha\alpha'}(t,t')\psi_{i\overline{\alpha}'}(t') - \frac{1}{4}\int_{-\infty}^{\infty} dt_1 dt_2 dt'_1 dt'_2 \sum_i \psi^*_{i\overline{\alpha}_1}(t_1)\psi^*_{i\overline{\alpha}_2}(t_2) \times \mathcal{G}^{2,c}_{i\alpha_1\alpha_2\alpha'_1\alpha'_2}(t_1,t_2,t'_1,t'_2)\psi_{i\overline{\alpha}'_1}(t'_1)\psi_{i\overline{\alpha}'_2}(t'_2). \tag{A12}$$

As pointed out in Ref. [59], the equilibrium action of the form in Eq. (A12) leads to the correct mean-field phase boundary, however it yields an unphysical excitation spectrum in the superfluid regime. This issue is circumvented by performing a second Hubbard-Stratonovich transformation [30, 59]. Starting from Eq. (A4) (keeping the source currents f this time), we introduce a second field z such that

$$e^{-\frac{i}{2}\int_{-\infty}^{\infty} dt \sum_{ij}(\psi^*_{i\overline{\alpha}}(t)+f^*_{i\overline{\alpha}}(t))[J]^{-1}_{ij}(\psi_{j\alpha}(t)+f_{j\alpha}(t))} = \int [\mathcal{D}z^*][\mathcal{D}z] e^{i\int_{-\infty}^{\infty} dt \sum_{ij} z^*_{i\overline{\alpha}}(t)(2J_{ij})z_{j\alpha}(t)} \times e^{iS_z[\psi]+iS_f[z]}, \tag{A13}$$

where

$$S_z[\psi] = \int_{-\infty}^{\infty} dt \sum_i z^{\overline{a}}_{i,\overline{\alpha}}(t)\psi^a_{i,\alpha}(t), \tag{A14}$$

so we may write $\mathcal{Z}[f]$ as

$$\mathcal{Z}[f] = \int [\mathcal{D}z^*][\mathcal{D}z] e^{i\int_{-\infty}^{\infty} dt \sum_{ij} z^*_{i\overline{\alpha}}(t)(2J_{ij})z_{j\alpha}(t)} \times e^{i\widetilde{W}[z]+iS_f[z]}, \tag{A15}$$

where

$$e^{i\widetilde{W}[z]} = \frac{1}{\mathcal{N}_\psi}\int [\mathcal{D}\psi^*][\mathcal{D}\psi] e^{iW_0[\psi]+iS_z[\psi]}, \tag{A16}$$

$$\mathcal{N}_\psi = \int [\mathcal{D}\psi^*][\mathcal{D}\psi] e^{iS^1_{\rm int}[\psi]}. \tag{A17}$$

By comparing Eq. (A15) to Eq. (12), we can see that the COGFs of the z field generated by $\mathcal{Z}[f]$ are identical to those of the bosonic field a.

The last step is to perform a cumulant expansion of $\widetilde{W}[z]$. The diagrams from this expansion can be categorized into two subsets: the "physical" diagrams and the "anomalous" diagrams [30, 59, 79]. In calculating the COGFs for the z fields from the generating function $\mathcal{Z}[f]$, the anomalous terms always cancel each other out, leaving only the physical diagrams [79]. Hence we can discard all the anomalous diagrams from the cumulant expansion. Keeping terms up to quartic order in the z fields we can write the generating functional $\mathcal{Z}[f]$ as

$$\mathcal{Z}[f] = \int [\mathcal{D}z^*][\mathcal{D}z] e^{iS_{\rm BHM}+iS_f[z]}, \tag{A18}$$

where $S_{\rm BHM}$ is given by Eq. (25).

Appendix B: Low frequency approximation

In the low frequency expression for the local Green's function, we introduced three parameters, υ, λ and κ^2. These were previously evaluated in Ref. [30] but are reproduced here for convenience. The parameters take the values (note that we defined λ with the opposite sign as compared to Ref. [30]):

$$\upsilon = \frac{Z}{\sum_{p=0}^{\infty} e^{-\beta(E_p-\mu p)}\left[\frac{(p+1)}{\mu-Up} - \frac{p}{\mu-U(p-1)}\right]}, \tag{B1}$$

$$\lambda = \frac{\upsilon^2}{Z}\sum_{p=0}^{\infty} e^{-\beta(E_p-\mu p)}\left[\frac{(p+1)}{[\mu-Up]^2} - \frac{p}{[\mu-U(p-1)]^2}\right], \tag{B2}$$

$$\kappa^2 = \frac{\lambda^2}{\upsilon} - \frac{\upsilon^2}{Z}\sum_{p=0}^{\infty} e^{-\beta(E_p-\mu p)} \times\left[\frac{(p+1)}{[\mu-Up]^3} - \frac{p}{[\mu-U(p-1)]^3}\right], \tag{B3}$$

where

$$Z = \sum_{p=0}^{\infty} e^{-\beta(E_p-\mu p)}.$$

The expressions for ν, λ and κ^2 simplify in the zero temperature limit:

$$\upsilon = \frac{(\mu-Un_0)(\mu-U(n_0-1))}{\mu+U},$$

$$\lambda = -\left[\frac{(2n_0-1)U-2\mu}{\mu+U} + \frac{(\mu-Un_0)(\mu-U(n_0-1))}{(\mu+U)^2}\right]$$

and

$$\kappa^2 = \frac{U^2 n_0(1+n_0)}{(U+\mu)^3}.$$

1. Four point vertex

The low frequency approximation to the four point vertex can be determined from the low frequency approximation for $u_{\alpha_1\alpha_2\alpha_3\alpha_4}(t_1,t_2,t_3,t_4)$. Starting from Eq. (26), make use of time translational invariance of the single site connected Green's function and take the low frequency approximation, which gives (noting that there is no contribution from the Keldysh Green's function except at points where the Mott lobes are degenerate)

$$u_{\alpha_1\alpha_2\alpha_3\alpha_4}(t_1,t_2,t_3,t_4) = -\left\{\left[\mathcal{G}^R\right]^{-1}(\omega=0)\right\}^4 \int \frac{d\omega_1}{2\pi}\frac{d\omega_2}{2\pi}\frac{d\omega_3}{2\pi}\frac{d\omega_4}{2\pi} e^{-i\omega_1 t_1 - i\omega_2 t_2 - i\omega_3 t_3 - i\omega_4 t_4}\mathcal{G}^{2,c}_{\overline{\alpha}_1\overline{\alpha}_2\overline{\alpha}_3\overline{\alpha}_4}(\omega_1,\omega_2,\omega_3,\omega_4). \tag{B4}$$

Explicit calculation of $\mathcal{G}^{2,c}_{\overline{\alpha}_1\overline{\alpha}_2\overline{\alpha}_3\overline{\alpha}_4}(\omega_1,\omega_2,\omega_3,\omega_4)$ followed by taking the low frequency limit leads to the two constants introduced in Eq. (64):

$$u_1 = -\frac{2\upsilon^4}{Z}\sum_{p=0}^{\infty} e^{-\beta\Delta_p}\left\{-\frac{(p+1)(p+2)}{\left[\Delta_p-\Delta_{p+2}\right]\left[\Delta_p-\Delta_{p+1}\right]^2} - \frac{p(p-1)}{\left[\Delta_p-\Delta_{p-2}\right]\left[\Delta_p-\Delta_{p-1}\right]^2} + \frac{(p+1)^2}{\left[\Delta_p-\Delta_{p+1}\right]^3} + \frac{p^2}{\left[\Delta_p-\Delta_{p-1}\right]^3} + \frac{p(p+1)}{\left[\Delta_p-\Delta_{p+1}\right]\left[\Delta_p-\Delta_{p-1}\right]^2} + \frac{p(p+1)}{\left[\Delta_p-\Delta_{p+1}\right]^2\left[\Delta_p-\Delta_{p-1}\right]}\right\}, \tag{B5}$$

and

$$u_2 = -\frac{i\upsilon^4}{Z}\sum_{p=0}^{\infty} e^{-\beta\Delta_p}\left[\frac{p+1}{[\Delta_p-\Delta_{p+1}]} + \frac{p}{[\Delta_p-\Delta_{p-1}]}\right]^2 + \frac{i\upsilon^4}{Z^2}\sum_{p=0}^{\infty}\sum_{q=0}^{\infty} e^{-\beta\Delta_p}e^{-\beta\Delta_q}\left[\frac{p+1}{[\Delta_p-\Delta_{p+1}]} + \frac{p}{[\Delta_p-\Delta_{p-1}]}\right]\left[\frac{q+1}{[\Delta_q-\Delta_{q+1}]} + \frac{q}{[\Delta_q-\Delta_{q-1}]}\right], \tag{B6}$$

where we used the notation $\Delta_p = E_p - \mu p$ and recalled the definition of υ in Eq. (59). Note that u_1 corresponds to the coefficient u introduced in Ref. [30], but u_2 is a coefficient that did not enter in that work, but is required to describe correlation function dynamics.

Appendix C: Equilibrium Green's functions in the one-loop approximation

In this appendix, we calculate the equilibrium Green's functions in the one-loop approximation. In order to obtain properly normalized spectral Green's functions, we do not apply any low-frequency approximation to the inverse bare propagator g_0^{-1}, however in order to obtain an analytical solution we approximate the interaction vertex $g^{a_1a_2a_3a_4}_{x_1x_2x_3x_4}$ by its static limit and drop all terms proportional to u_2

$$g^{a_1a_2a_3a_4}_{x_1x_2x_3x_4} = -u_1\delta(t_1-t_2)\delta(t_1-t_3)\delta(t_1-t_4)\zeta^{a_1a_2a_3a_4}_{\alpha_1\alpha_2\alpha_3\alpha_4}, \tag{C1}$$

where $\zeta^{a_1a_2a_3a_4}_{\alpha_1\alpha_2\alpha_3\alpha_4}$ was defined in Eq. (65).

We also focus on the zero-temperature case so that an analytical solution can be obtained. Note that in determining initial conditions there is no quench so the hopping term is time independent:

$$J^{a_1a_2}_{ij,x_1x_2} = \sigma_1^{a_1a_2}\tau^1_{\alpha_1\alpha_2}\delta(t_1-t_2)\begin{cases}\frac{1}{2}J, & i,j \text{ nearest neighbours}\\ 0, & \text{otherwise}\end{cases}. \tag{C2}$$

We consider Eq. (50) to zero-loop order (i.e. make the mean-field approximation), giving

$$\frac{\delta S[\phi]}{\delta\phi^{a_1}_{i,x_1}} = 0, \tag{C3}$$

which leads to

$$\sum_j\left(\delta_{ij}\left[\mathcal{G}^{-1}\right]^{a_1a_2}_{x_1x_2} + 2J^{a_1a_2}_{ij,x_1x_2}\right)\phi^{a_2}_{j,x_2} + \frac{1}{3!}g^{a_1a_2a_3a_4}_{x_1x_2x_3x_4}\phi^{a_2}_{i,x_2}\phi^{a_3}_{i,x_3}\phi^{a_4}_{i,x_4} = 0. \tag{C4}$$

Acting on both sides with $\delta_{ij}\mathcal{G}^{a_1a_2}_{x_1x_2}$ yields

$$\phi^{a_1}_{i,x_1} + \sum_j\delta_{ij}\mathcal{G}^{a_1a_2}_{x_1x_2}\left(\sum_k 2J^{a_2a_3}_{jk,x_2x_3}\phi^{a_3}_{k,x_3} + \frac{1}{3!}g^{a_2a_3a_4a_5}_{x_2x_3x_4x_5}\phi^{a_3}_{j,x_3}\phi^{a_4}_{j,x_4}\phi^{a_5}_{j,x_5}\right) = 0, \tag{C5}$$

and setting $a_1 = 2$, $\alpha_1 = q$, Eq. (C5) becomes

$$\phi + \upsilon^{-1}\left((zJ)\phi - u_1\phi^3\right) = 0, \tag{C6}$$

which can be solved for ϕ to yield

$$\phi = \begin{cases}\sqrt{\frac{\upsilon+zJ}{u_1}} & \text{if } zJ > -\upsilon\\ 0 & \text{otherwise}\end{cases}, \tag{C7}$$

where we assumed that ϕ was real without loss of generality. Next we calculate G from Eq. (51) to one-loop order by dropping the 2PI self-energy term

$$\left[G^{-1}\right]^{a_1a_2}_{ij,x_1x_2} = \delta_{ij}\left[\mathcal{G}^{-1}\right]^{a_1a_2}_{x_1x_2} + 2J^{a_1a_2}_{ij,x_1x_2} + \frac{1}{2}\delta_{ij}g^{a_1a_2a_3a_4}_{x_1x_2x_3x_4}\phi^{a_3}_{i,x_3}\phi^{a_4}_{i,x_4}. \tag{C8}$$

Define the one-loop self-energy $\Sigma^{a_1a_2,(1)}_{ij,x_1x_2}$ as

$$\Sigma^{a_1a_2,(1)}_{ij,x_1x_2} = -\frac{1}{2}\delta_{ij}g^{a_1a_2a_3a_4}_{x_1x_2x_3x_4}\phi^{a_3}_{i,x_3}\phi^{a_4}_{i,x_4}, \tag{C9}$$

then Eq. (C8) can be rewritten as

$$G^{a_1a_2}_{ij,x_1x_2} = \delta_{ij}\mathcal{G}^{a_1a_2}_{x_1x_2} + \mathcal{G}^{a_1a_3}_{x_1x_3}\left(-2J^{a_3a_4}_{ij,x_3x_4} + \Sigma^{a_3a_4,(1)}_{ij,x_3x_4}\right)\mathcal{G}^{a_4a_2}_{x_4x_2}. \tag{C10}$$

At this point, we could generate a coupled set of equations for $G^{21,(R)}$ and $G^{11,(R)}$ by setting $(a_1,a_2,\alpha_1,\alpha_2)$ in Eq. (C10) to $(2,1,c,q)$ and $(1,1,c,q)$ respectively. The easiest way to solve these equations is by working in momentum-frequency

space, where we can obtain an analytical solution. Once we have calculated $G^{21,(R)}_{\mathbf{k}}(\omega)$ and $G^{11,(R)}_{\mathbf{k}}(\omega)$, we can calculate the spectral fucntions using the following relations

$$\rho^{(\rho)}_{\mathbf{k}}(\omega) = -2\,\mathrm{Im}\left[G^{21,(R)}_{\mathbf{k}}(\omega)\right], \qquad m^{(\rho)}_{\mathbf{k}}(\omega) = -2\,\mathrm{Im}\left[G^{11,(R)}_{\mathbf{k}}(\omega)\right], \tag{C11}$$

and then perform the inverse Fourier transform to obtain $\rho^{(\rho)}_{ij}(t_1,t_2)$ and $m^{(\rho)}_{ij}(t_1,t_2)$. Lastly, to calculate $\rho^{(F)}_{ij}(t_1,t_2)$ and $m^{(F)}_{ij}(t_1,t_2)$ we use the fluctuation-dissipation theorem [87]

$$\rho^{(F)}_{ij}(\omega) = \frac{1}{2\pi}\mathcal{P}\int_{-\infty}^{\infty} dt' \rho^{(\rho)}_{ij}(t')\frac{1}{t'-t}, \qquad m^{(F)}_{ij}(\omega) = \frac{1}{2\pi}\mathcal{P}\int_{-\infty}^{\infty} dt' m^{(\rho)}_{ij}(t')\frac{1}{t'-t}, \tag{C12}$$

where $\mathcal{P}$ indicates the principal value of the integral.

In the Mott insulator regime, we have

$$m^{(\rho)}_{ij}(t_1,t_2) = 0, \tag{C13}$$

$$m^{(F)}_{ij}(t_1,t_2) = 0, \tag{C14}$$

and

$$\rho^{(\rho)}_{ij}(t_1,t_2) = -\tfrac{1}{N_s}\textstyle\sum_{\mathbf{k}} \frac{\cos[\mathbf{k}\cdot(\mathbf{r}_i-\mathbf{r}_j)]}{E^+_{\mathbf{k}}-E^-_{\mathbf{k}}}\left\{e^{-iE^+_{\mathbf{k}}(t-t')}\left[E^+_{\mathbf{k}}-(U+\mu)\right] - e^{-iE^-_{\mathbf{k}}(t-t')}\left[E^-_{\mathbf{k}}-(U+\mu)\right]\right\}, \tag{C15}$$

$$\rho^{(F)}_{ij}(t_1,t_2) = \tfrac{i}{2N_s}\textstyle\sum_{\mathbf{k}} \frac{\cos[\mathbf{k}\cdot(\mathbf{r}_1-\mathbf{r}_2)]}{E^+_{\mathbf{k}}-E^-_{\mathbf{k}}}\left\{e^{-iE^+_{\mathbf{k}}(t-t')}\left[E^+_{\mathbf{k}}-(U+\mu)\right] + e^{-iE^-_{\mathbf{k}}(t-t')}\left[E^-_{\mathbf{k}}-(U+\mu)\right]\right\}, \tag{C16}$$

where

$$E^{\pm}_{\mathbf{k}} \equiv \frac{\tilde{A}_{\mathbf{k}}}{2} \pm \frac{1}{2}\sqrt{\tilde{A}^2_{\mathbf{k}} - 4\tilde{B}_{\mathbf{k}}}, \tag{C17}$$

$$\tilde{A}_{\mathbf{k}} \equiv (\mu - Un_0) + (\mu - U(n_0-1)) + 2\epsilon_{\mathbf{k}}, \tag{C18}$$

$$\tilde{B}_{\mathbf{k}} \equiv (U+\mu)(\upsilon + 2\epsilon_{\mathbf{k}}), \tag{C19}$$

$$\epsilon_{\mathbf{k}} \equiv \sum_i e^{-i\mathbf{k}\cdot\mathbf{r}_i} J_{ij} = J\sum_{n=1}^{d}\cos(k_n a), \tag{C20}$$

with $n_0 \equiv n_0(\mu)$ the (integer) number of bosons per site in the local limit at $T=0$ for chemical potential μ, a is the lattice constant, and υ is given in Appendix B.

Appendix D: Equations of motion in the MI regime

Here we explicitly write the equations of motion of the low-frequency approximation in the MI regime to second order in u. Note that in the MI regime, $\phi = m^{(\rho,F)} = 0$. To write the equations of motions more compactly, we introduce the following notation

$$F_{ij,12} = F_{ij}(t_1,t_2), \tag{D1}$$

where F is an arbitrary function. Furthermore, following Ref. [70], we introduce (for functions $\mathbf{f}$ and $\mathbf{g}$)

$$\Omega^{(F)}_{ij,12}[\mathbf{f},\mathbf{g}] = \mathbf{f}^{(F)}_{ij}(t_1,t_2)\mathbf{g}^{(F)}_{ij}(t_1,t_2) - \frac{1}{4}\left[\mathbf{f}^{(\rho)}_{ij}(t_1,t_2)\mathbf{g}^{(\rho)}_{ij}(t_1,t_2)\right], \tag{D2}$$

$$\Omega^{(\rho)}_{ij,12}[\mathbf{f},\mathbf{g}] = \mathbf{f}^{(F)}_{ij}(t_1,t_2)\mathbf{g}^{(\rho)}_{ij}(t_1,t_2) + \mathbf{f}^{(\rho)}_{ij}(t_1,t_2)\mathbf{g}^{(F)}_{ij}(t_1,t_2), \tag{D3}$$

$$\Delta^{(\rho,F)}_{ij,12} = \Omega^{(\rho,F)}_{ij,12}[\rho,\rho^*] + 2\Omega^{(\rho,F)}_{ij,12}[m,m^*], \tag{D4}$$

$$\Upsilon^{(\rho,F)}_{ij,12} = 2\Omega^{(\rho,F)}_{ij,12}[\rho,\rho^*] + \Omega^{(\rho,F)}_{ij,12}[m,m^*]. \tag{D5}$$

The equations of motion can then be written in the following form

$$\left(\upsilon - i\lambda\partial_{t_1} - \kappa^2\partial_{t_1}^2\right)\rho_{ij}^{(F)}(t_1,t_2) = -2\sum_k J_{ik}(t_1)\rho_{kj}^{(F)}(t_1,t_2) + 2iu_1\rho_{ii}^{(F)}(t_1,t_1)\rho_{ij}^{(F)}(t_1,t_2)$$
$$+u_2\int_{t_0}^{t_1} dt_3\rho_{ii}^{(\rho)}(t_1,t_3)\rho_{ij}^{(F)}(t_3,t_2) - u_2\int_{t_0}^{t_2} dt_3\rho_{ii}^{(F)}(t_1,t_3)\rho_{ij}^{(\rho)}(t_3,t_2)$$
$$-2iu_1^2\sum_k\int_{t_0}^{t_1} dt_3\Omega_{ik,13}^{(\rho)}[\rho,\Delta]\rho_{kj,32}^{(F)} + 2iu_1^2\sum_k\int_{t_0}^{t_2} dt_3\Omega_{ik,13}^{(F)}[\rho,\Delta]\rho_{kj,32}^{(\rho)}, \quad \text{(D6)}$$

and

$$\left(\upsilon - i\lambda\partial_{t_1} - \kappa^2\partial_{t_1}^2\right)\rho_{ij}^{(\rho)}(t_1,t_2) = -2\sum_k J_{ik}(t_1)\rho_{kj}^{(\rho)}(t_1,t_2) + 2iu_1\rho_{ii}^{(F)}(t_1,t_1)\rho_{ij}^{(\rho)}(t_1,t_2)$$
$$+u_2\int_{t_2}^{t_1} dt_3\rho_{ii}^{(\rho)}(t_1,t_3)\rho_{ij}^{(\rho)}(t_3,t_2) - 2iu_1^2\sum_k\int_{t_2}^{t_1} dt_3\Omega_{ik,13}^{(\rho)}[\rho,\Delta]\rho_{kj,32}^{(\rho)}. \quad \text{(D7)}$$

[1] I. Bloch, Nature Phys. **1**, 23 (2005); D. Jaksch and P. Zoller, Ann. Phys. **315**, 52 (2005).
[2] O. Morsch and M. Oberthaler, Rev. Mod. Phys. **78**, 179 (2006).
[3] M. Lewenstein, A. Sanpera, V. Ahufinger, B. Damski, A. Sen, and U. Sen, Adv. Phys. **56**, 243 (2007).
[4] I. Bloch, J. Dalibard, and W. Zwerger, Rev. Mod. Phys. **80**, 885 (2008).
[5] M. P. Kennett, ISRN Condensed Matter Physics, **2013**, 393616 (2013).
[6] M. P. A. Fisher, P. B. Weichman, G. Grinstein, and D. S. Fisher, Phys. Rev. B **40**, 546 (1989).
[7] D. Jaksch, C. Bruder, J. I. Cirac, C. W. Gardiner, P. Zoller, Phys. Rev. Lett. **81**, 3108 (1998).
[8] M. Greiner, O. Mandel, T. Esslinger, T. W. Hansch, and I. Bloch, Nature **415**, 39 (2002).
[9] M. Greiner, M. O. Mandel, T. Hänsch, and I. Bloch, Nature **419**, 51 (2002).
[10] T. Stöferle, H. Moritz, C. Schori, M. Köhl, and T. Esslinger, Phys. Rev. Lett. **92**, 130403 (2004).
[11] C. Schori, T. Stöferle, H. Moritz, M. Köhl, and T. Esslinger, Phys. Rev. Lett. **93**, 240402 (2004).
[12] M. Köhl, H. Moritz, T. Stöferle, C. Schori, and T. Esslinger, J. Low Temp. Phys. **138**, 635 (2005).
[13] F. Gerbier, A. Widera, S. Fölling, O. Mandel, T. Gericke, and I. Bloch, Phys. Rev. A **72**, 053606 (2005).
[14] F. Gerbier, A. Widera, S. Fölling, O. Mandel, T. Gericke, and I. Bloch, Phys. Rev. Lett. **95**, 050404 (2005).
[15] I. B. Spielman, W. D. Phillips, and J. V. Porto, Phys. Rev. Lett. **98**, 080404 (2007).
[16] I. B. Spielman, W. D. Phillips, and J. V. Porto, Phys. Rev. Lett. **100**, 120402 (2008).
[17] W. S. Bakr, A. Peng, M. E. Tai, R. Ma, J. Simon, J. I. Gillen, S. Fölling, L. Pollet, and M. Greiner, Science **329**, 547 (2010).
[18] K. Jiménez-García, R. L. Compton, Y.-J. Lin, W. D. Phillips, J. V. Porto, and I. B. Spielman, Phys. Rev. Lett. **105**, 110401 (2010).
[19] J. F. Sherson, C. Weitenberg, M. Endres, M. Cheneau, I. Bloch, and S. Kuhr, Nature **467**, 68 (2010).
[20] S. Trotzky, L. Pollet, F. Gerbier, U. Schorrberger, I. Bloch, N. V. Prokof'ev, B. Svistunov, and M. Troyer, Nature Phys. **6**, 998 (2010).
[21] S. Will, T. Best, U. Schneider, L. Hackermüller, D.-S. Lühmann, and I. Bloch, Nature **465**, 197 (2010).
[22] D. Chen, M. White, C. Borries, and B. De Marco, Phys. Rev. Lett. **106**, 235304 (2011).
[23] S. Trotzky, Y.-A. Chen, A. Flesch, I. P. McCulloch, U. Schollwöck, J. Eisert, and I. Bloch, Nature Phys. **8**, 325 (2012).
[24] K. W. Mahmud, L. Jiang, P. R. Johnson, and E. Tiesinga, New J. Phys. **16**, 103009 (2014).
[25] C. Kollath, A. M. Läuchli, and E. Altman, Phys. Rev. Lett. **98**, 180601 (2007).
[26] U. R. Fischer, R. Schützhold, and M. Uhlmann, Phys. Rev. A **77**, 043615 (2008).
[27] U. R. Fischer and R. Schützhold, Phys. Rev. A **78**, 061603 (2008).
[28] B. Sciolla and G. Biroli, Phys. Rev. Lett. **105**, 220401 (2010).
[29] B. Sciolla and G. Biroli, J. Stat. Mech. **11**, 11003 (2011).
[30] M. P. Kennett and D. Dalidovich, Phys. Rev. A **84**, 033620 (2011).
[31] H. U. R. Strand, M. Eckstein, and P. Werner, Phys. Rev. X **5**, 011038 (2015).
[32] I. S. Landea and N. Nessi, Phys. Rev. A **91**, 063601 (2015).
[33] T. W. B. Kibble, J. Phys. A **9**, 1387 (1976).
[34] W. H. Zurek, Nature **317**, 505 (1985).
[35] W. H. Zurek, U. Dorner, and P. Zoller, Phys. Rev. Lett. **95**, 105701 (2005).
[36] A. Polkovnikov, Phys. Rev. B **72**, 161201(R) (2005).
[37] V. Gritsev and A. Polkovnikov, in *Understanding Quantum Phase Transitions* ed. L. D. Carr (Taylor and Francis, Boca Raton, 2010).
[38] G. G. Batrouni, V. Rousseau, R. T. Scalettar, M. Rigol, A. Muramatsu, P. J. H. Denteneer, and M. Troyer, Phys. Rev. Lett. **89**, 117203 (2002).
[39] B. DeMarco, C. Lannert, S. Vishveshwara, and T.-C. Wei, Phys. Rev. A **71**, 063601 (2005).

[40] S. S. Natu, K. R. A. Hazzard, E. J. Mueller, Phys. Rev. Lett. **106**, 125301 (2011).

[41] J. S. Bernier, G. Roux, and C. Kollath, Phys. Rev. Lett. **106**, 200601 (2011).

[42] C.-L. Hung, X. Zhang, N. Gemelke, and C. Chin, Phys. Rev. Lett. **104**, 160403 (2010).

[43] A. Dutta, R. Sensarma, and K. Sengupta, arXiv:1406.0849v2.

[44] E. H. Lieb and D. W. Robinson, Commun. Math. Phys. **28**, 251 (1972).

[45] A. Läuchli and C. Kollath, J. Stat. Mech P05018 (2008).

[46] P. Barmettler, D. Poletti, M. Cheneau, and C. Kollath, Phys. Rev. A **85**, 053625 (2012).

[47] M. Cheneau, P. Barmettler, D. Poletti, M. Endres, P. Schauβ, T. Fukuhara, C. Gross, I. Bloch, C. Kollath, and S. Kuhr, Nature **481**, 484 (2012).

[48] P. Navez and R. Schützhold, Phys. Rev. A **82**, 063603 (2010).

[49] S. S. Natu, and E. J. Mueller, Phys. Rev. A **87**, 063616 (2013).

[50] J.-S. Bernier, D. Poletti, P. Barmettler, G. Roux, and C. Kollath, Phys. Rev. A **85**, 033641 (2012).

[51] S. R. Clark and D. Jaksch, Phys. Rev. A **70**, 043612 (2004).

[52] J. Zakrzewski, Phys. Rev. A **71**, 043601 (2005).

[53] L. Amico and V. Penna, Phys. Rev. B **62**, 1224 (2000).

[54] C. Schroll, F. Marquardt, and C. Bruder, Phys. Rev. A **70**, 053609 (2004).

[55] C. Trefzger and K. Sengupta, Phys. Rev. Lett. **106**, 095702 (2011).

[56] A. Dutta, C. Trefzger, and K. Sengupta, Phys. Rev. B **86**, 085140 (2012).

[57] Y. Yanay and E. J. Mueller, Phys. Rev. A **93**, 013622 (2016).

[58] F. Queisser, K. V. Krutitsky, P. Navez, and R. Schützhold, Phys. Rev. A **89**, 033616 (2014).

[59] K. Sengupta and N. Dupuis, Phys. Rev. A **71**, 033629 (2005).

[60] J. Schwinger, J. Math. Phys **2**, 407 (1961).

[61] L. V. Keldysh, Zh. Eksp. Teor. Fiz. **47**, 1515 (1964) [Sov. Phys. JETP **20**, 1018 (1965)].

[62] J. Rammer and H. Smith, Rev. Mod. Phys. **58**, 323 (1986).

[63] A. J. Niemi and G. W. Semenoff, Ann. Phys. **152**, 105 (1984).

[64] N. P. Landsman and C. G. van Weert, Phys. Rep. **145**, 141 (1987).

[65] K.-C. Chou, Z.-B. Su, B.-L. Hao, and L. Yu, Phys. Rep. **118**, 1 (1985).

[66] A. Robertson, V. M. Galitski, and G. Refael, Phys. Rev. Lett. **106**, 165701 (2011).

[67] T. D. Graβ, F. E. A. dos Santos, and A. Pelster, Laser Phys. **21**, 1459 (2011).

[68] T. D. Graβ, F. E. A. dos Santos, and A. Pelster, Phys. Rev. A **84**, 013613 (2011).

[69] T. D. Graβ, diploma thesis (Freie Universität Berlin, 2009).

[70] A. M. Rey, B. L. Hu, E. Calzetta, A. Roura, and C. W. Clark, Phys. Rev. A **69**, 033610 (2004).

[71] A. M. Rey, B. L. Hu, E. Calzetta, and C. W. Clark, Phys. Rev. A **72**, 023604 (2005).

[72] K. Temme and T. Gasenzer, Phys. Rev. A **74**, 053603 (2006).

[73] E. Calzetta, B. L. Hu, and A. M. Rey, Phys. Rev. A **73**, 023610 (2006).

[74] A. Polkovnikov, Phys. Rev. A **68**, 053604 (2003).

[75] J. W. Negele and H. Orland, *Quantum Many Particle Systems* (Addison-Wesley, Reading, MA, 1998).

[76] M. A. van Eijck, R. Kobes, and Ch. G. van Weert, Phys. Rev. D **50**, 4097 (1994).

[77] L. F. Cugliandolo and G. Lozano, Phys. Rev. B **59**, 915 (1999).

[78] M. P. Kennett, C. Chamon, and J. Ye, Phys. Rev. B **64**, 224408 (2001).

[79] N. Dupuis, Nucl. Phys. B **618**, 617 (2001).

[80] J. Rammer, *Quantum Field Theory of Non-equilibrium States* (Cambridge University Press, New York, NY, 2007).

[81] J. M. Cornwall, R. Jackiw, and E. Tomboulis, Phys. Rev. D **10**, 2428 (1974).

[82] J. Berges and J. Cox, Phys. Lett. B **517**, 369 (2001); G. Aarts and J. Berges, Phys. Rev. D **64**, 105010 (2001); G. Aarts, D. Ahrensmeier, R. Baier, J. Berges, and J. Serreau, Phys. Rev. D **66**, 045008 (2002); J. Berges, Nucl. Phys. A **699**, 847 (2002).

[83] L. P. Kadanoff and G. Baym, *Quantum Statistical Mechanics: Green's function Methods in Equilibrium and Nonequilibrium Problems* (Addison-Wesley, New York, 1962).

[84] W. Zwerger, J. Opt. B: Quantum Semiclass. Opt. **5**, S9 (2003).

[85] D. Sen, K. Sengupta, and S. Mondal, Phys. Rev. Lett. **101**, 016806 (2008).

[86] D. Dalidovich and M. P. Kennett, Phys. Rev. A **79**, 053611 (2009).

[87] N. Pottier, Physica A **291**, 327-344 (2001).